Nano Research
2022, 15(8): 7139–7153

ISSN 1998-0124 CN 11-5974/O4
https://doi.org/10.1007/s12274-022-4322-6

Review Article

Progress toward understanding the fullerene-related chemical interactions in perovskite solar cells

Kaikai Liu, Chengbo Tian (✉), Yuming Liang, Yujie Luo, Liqiang Xie, and Zhanhua Wei (✉)

Xiamen Key Laboratory of Optoelectronic Materials and Advanced Manufacturing, Institute of Luminescent Materials and Information Displays, College of Materials Science and Engineering, Huaqiao University, Xiamen 361021, China

Received: 27 January 2022 / **Revised:** 11 March 2022 / **Accepted:** 13 March 2022

ABSTRACT

Fullerene materials have been widely used to fabricate efficient and stable perovskite solar cells (PSCs) due to their excellent electron transport ability, defect passivation effect, and beyond. Recent studies have shown that fullerene-related chemical interaction has played a crucial role in determining device performance. However, the corresponding fullerene-related chemical interactions are yet well understood. Herein, a comprehensive review of fullerene materials in regulating carrier transport, passivating the surface and grain boundary defects, and enhancing device stability is provided. Specifically, the influence of the fullerene-related chemical interactions, including fullerene-perovskite, fullerene-inorganic electron transport layer (IETL), and fullerene-fullerene, on the device performance is well discussed. Finally, we outline some perspectives for further design and application of fullerene materials to enhance the performance and commercial application of PSCs.

KEYWORDS

perovskite solar cells, functional fullerenes, chemical interactions, device performance

1 Introduction

Organic–inorganic halide perovskite materials, which adopt the structure of ABX_3 (Fig. 1(a)), have excellent optoelectronic properties, such as high absorption coefficient, tunable and suitable optical bandgap, small exciton binding energy, and high carrier mobility [1–5]. Benefiting from these exceptional properties of the perovskite materials and well-established solar cell manufacturing technology from organic solar cells (OSCs) and dye-sensitized solar cells (DSSCs), the power conversion efficiency (PCE) of perovskite solar cells (PSCs) has been increased from the origin of 3.8% to the certified value of 25.7% in about one decade [6–12]. Therefore, the PSCs have become one of the most promising candidates for the next generation photovoltaic [13–18].

However, there is still a long way to improve the PSC efficiency towards its theoretical Shockley–Queisser (S–Q) efficiency limit of more than 30% and to enhance the stability towards commercial application [19]. In the past years, many works aiming to improve PCE and device stability have been carried out, which are involved in component and interface engineering, development of new carrier transport materials, and device structure optimization [20–30]. Among these contributions, fullerene materials also greatly promote the device performances due to their special physical and chemical properties, such as high electron affinity, excellent electron mobility, good hydrophobicity, and defect passivation effect [31–34].

The original fullerenes represented by C_{60} and C_{70} can be chemically modified to form different functionalized fullerene derivatives, such as the most commonly used [6,6]-phenyl-C_{61}-butyric acid methyl ester (PCBM) and the C_{70} based analog ($PC_{71}BM$) (Fig. 1(b)), thereby effectively expanding the members of the fullerene family [35, 36]. Meanwhile, the easy solution processability of fullerene materials makes them be used in both inverted and normal architecture devices. As shown in Fig. 1(c), fullerenes can be used as various type functions in PSCs, such as (1) electron transport layer (ETL) to extract and transport electrons to the corresponding electrode; (2) interfacial layer to reduce the surface defects of the upper or the underlying layers to suppress carrier recombination; (3) fullerene-perovskite bulk-heterojunction to improve the film quality of perovskite and reduce the bulk defects within perovskite films [37–41]. Besides, fullerene can also be used as an encapsulation layer, a hydrophobic interfacial layer, and lead-leakage prevention materials to enhance the device stability and practicality [42–45]. Furthermore, with more and more fullerene derivatives being synthesized and applied in PSCs, the efficiency of fullerene-based devices has been quickly improved. As shown in Fig. 1(d), we summarized the efficiency evolution process of fullerene-based inverted and normal configuration PSCs in recent years. To date, the inverted architecture PSCs with fullerene as the ETLs have made great progress in the past years, with a certified efficiency exceeding 24% [46]. The efficiency gap between the inverted and normal configuration PSCs is getting smaller [12, 46].

More importantly, it is found that the chemical interactions of fullerene–fullerene and fullerene–adjacent material significantly impact device performance. Therefore, it is urgent to systematically investigate and summarize the effects of fullerene-related chemical interactions in the PSCs. Here, we provide a development overview of fullerene-related chemical interactions

Address correspondence to Chengbo Tian, cbtian@hqu.edu.cn; Zhanhua Wei, weizhanhua@hqu.edu.cn

for fabricating efficient and stable PSCs. We not only introduce the advantages and roles of fullerene materials but also summarize the effect of three types of chemical interactions, including the interactions between fullerene and perovskite interface (fullerene–perovskite), the interactions between fullerene and inorganic electron transport layer (fullerene–IETL), and the interactions between fullerene molecules (fullerene–fullerene). It is different from previous reviews that mainly focused on the functions of fullerenes and the photovoltaic performance of different fullerene materials [31, 40, 47, 48]. Finally, we propose an outlook in designing functional fullerenes to improve the photovoltaic performances of PSCs.

2 The roles of fullerenes in perovskite solar cells

The roles of fullerene materials in PSCs can be divided into electron extraction and transport, defect passivation, and device stability enhancement. Firstly, fullerene materials are one of the best candidates for electron transport materials due to their suitable energy levels and high electron mobilities. Secondly, fullerene materials have an efficient passivation effect for the perovskite surface and grain boundary defects. Finally, fullerene materials can effectively improve the stability of the devices due to their hydrophobic characteristics and inhibition of ion migration properties.

2.1 Fullerenes act as electron transport materials in PSCs

With high electron affinity and electron mobility, fullerene materials are widely regarded as excellent electron extraction and transport materials. In 2013, Jeng et al. first employed fullerenes as the ETLs to fabricate the inverted PSCs (Fig. 2(a)) [49]. They found that the lowest unoccupied molecular orbital (LUMO) energy level of $CH_3NH_3PbI_3$ perovskite is located at −3.9 eV, which matched well with the LUMO energy level of −3.9 eV of PCBM. As shown in Fig. 2(b), when a PSC is under illumination, photo-generated electrons/holes in the perovskite layer are produced, then transferred to the corresponding carriers transporting layers and collected by the electrodes to complete the process of photoelectric conversion. The spectral response of the device also showed that the main photocurrent comes from the $CH_3NH_3PbI_3$ perovskite layer (Fig. 2(c)). As a result, the as-fabricated PSCs containing PCBM as the ETL yielded a promising PCE of 3.9% (V_{OC} = 0.60 V, J_{SC} =

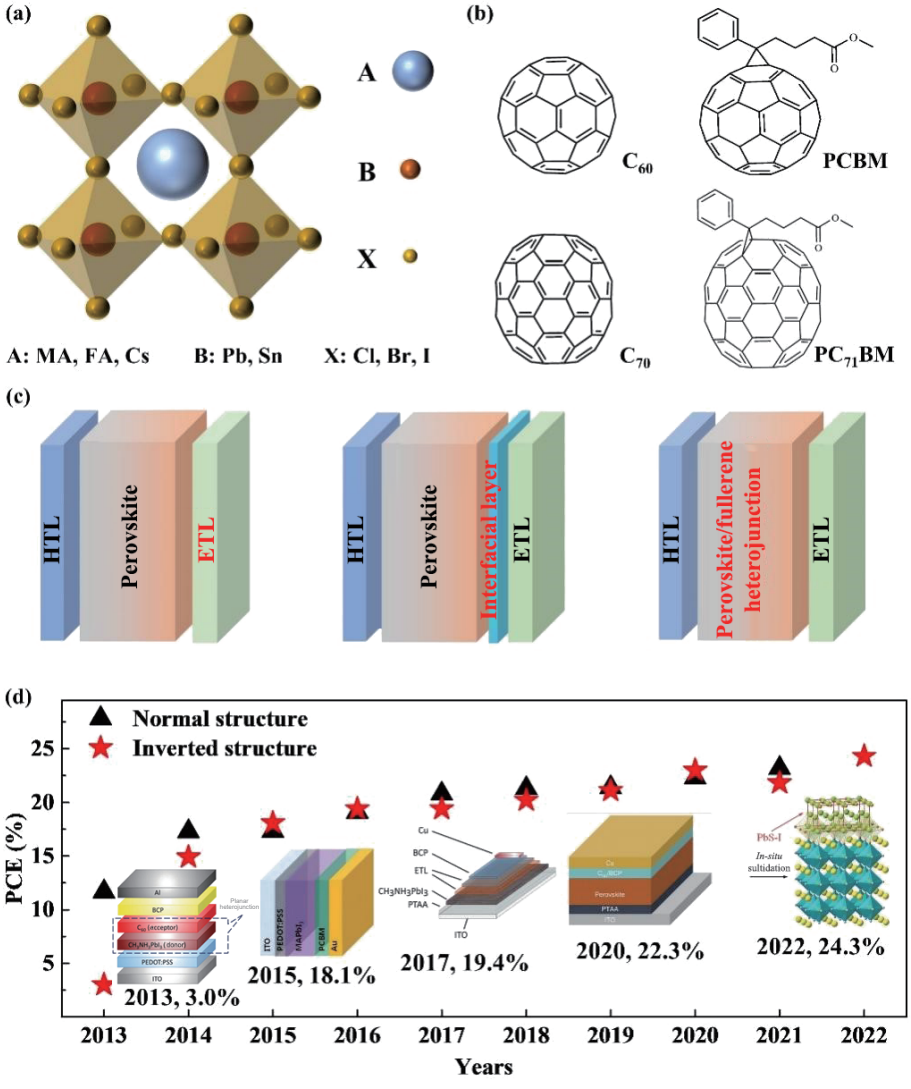

Figure 1 (a) Schematic diagram of the perovskite materials with a structure of ABX_3. (b) Structure model diagram of the fullerenes: C_{60}, C_{70}, PCBM, and $PC_{71}BM$. (c) Schematic diagram of the application of fullerene materials in PSCs, including the inverted and normal configurations. (d) Summary of the efficiency evolution process of fullerene-based inverted and normal configuration PSCs (reproduced with permission from Ref. [49], © WILEY-VCH Verlag GmbH & Co. KGaA, Weinheim 2013; reproduced with permission from Ref. [50], © The Royal Society of Chemistry 2015; reproduced with permission from Ref. [51], © WILEY-VCH Verlag GmbH & Co. KGaA, Weinheim 2017; reproduced with permission from Ref. [33], © Zheng, X. P. et al. 2020; reproduced with permission from Ref. [46], © Li, X. D. et al. 2022).

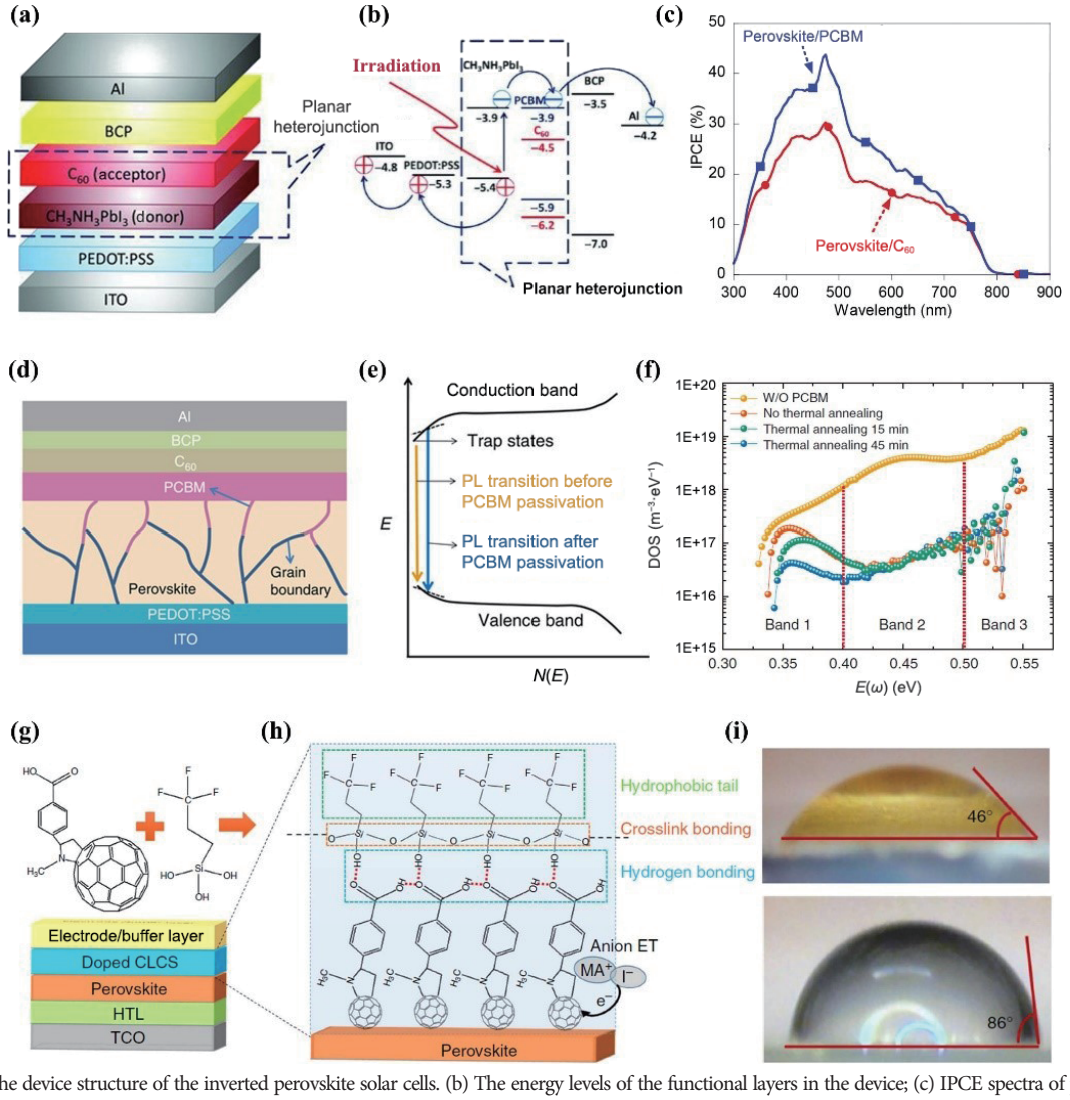

Figure 2 (a) The device structure of the inverted perovskite solar cells. (b) The energy levels of the functional layers in the device; (c) IPCE spectra of perovskite/C_{60}-based and perovskite/PCBM-based devices. Reproduced with permission from Ref. [49], © WILEY-VCH Verlag GmbH & Co. KGaA, Weinheim 2013. (d) Schematic diagram of the diffusion of PCBM molecules along the perovskite grain boundaries. (e) Schematic of PL peaks with a blue-shift from passivation effect of the PCBM. (f) The recorded trap density of states (tDOS) from the thermal admittance spectroscopy. Reproduced with permission from Ref. [52], © Macmillan Publishers Limited 2014. (g) Schematic illustration of the C_{60}-SAM with a silane coupling agent and the device structure with the cross-linked C_{60}-SAM as ETLs. (h) Schematic illustration for the crosslinking of C_{60}-SAM with a silane-coupling agent. (i) Contact angles of water on the non-crosslinked C_{60}-SAM film (upper) and crosslinked C_{60}-SAM film (bottom). Reproduced with permission from Ref. [53], © Bai, Y. et al. 2016.

10.32 mA·cm^{-2}, and fill factor (FF) = 0.63), suggesting the fullerenes are promising ETL materials for fabricating PSCs.

Since then, the PSCs with fullerene materials serve as ETLs achieved rapid development by constructing new device structures [23, 40, 54–56]. For instance, the LUMO energy level of PCBM is located between the LUMO energy level of perovskite film (–3.75 eV) and TiO_x layer (–4.0 eV), which can enhance the electron transport. Thus the device based on PCBM/TiO_x yielded an improved device efficiency of 10% [57]. Similarly, Xie et al. introduced the [6,6]-phenyl-C_{61}-butyric acid 2-((2-(dimethylamino) -ethyl) (methyl)amino)ethyl ester (PCBDAN) film between the indium tin oxide (ITO) and PCBM layer to reduce the interfacial barriers [38]. The double layer of PABDAN/PCBM can reduce the work functions (WFs) of the ITO layer to enhance the charge extraction and decrease the recombination loss, yielding a PCE of 18.1%. Cao et al. synthesized a water-soluble fullerene derivative, $C_{60}O_{\sim 18}(OH)_{\sim 10}(NH_2)_{\sim 8}$ (F-C_{60}), and incorporated it into PSCs [58]. Since the deeper work function of F-C_{60}, it was used as modifying layer between the ITO and C_{60} ETL to construct a gradient energy level, thereby reducing the energy loss for transporting the charge carriers.

Except for the C_{60}-based fullerene materials, C_{70}-based derivatives were also used as ETLs or modification layers in the PSCs. Xing et al. synthesized various hydrophilic fullerene derivatives with electron-rich groups and applied them as ETLs in the PSCs [59]. They demonstrated that the electron-rich group of fullerene derivatives reduced the WF of the metal cathode and improved the charge transport capacity of the interface between perovskite and electrode. Thus, the final device yielded a high PCE of 16%. Dai et al. precisely tuned the ratio of the three isomers of the $PC_{71}BM$ layer and obtained a smooth film with negligible molecular aggregations [60]. As a result, the device reached a high PCE of 17.56%.

To sum up, it can be concluded that the fullerene and its derivatives are a class of excellent electron transport materials for both normal and inverted configuration PSCs.

2.2 Fullerenes as passivators in PSCs

The prevailing solution-process in fabricating perovskite films usually generated an amount of unexcepted charge traps at the surfaces and grain boundaries of perovskite films defects, which resulted in the notorious current–voltage hysteresis and poor device performance. As shown in Figs. 2(d) and 2(e), Shao et al. deposited a PCBM layer on the surface of the perovskite layer and

found that the PCBM film efficiently passivated the traps of the top surface of perovskite film by showing the obvious photoluminescence (PL) transition with a blue shift [52]. Moreover, the permeated PCBM molecules along the grain boundaries of perovskite effectively passivated the shallow traps and deep traps (Fig. 2(f)). Benefiting from the passivation of PCBM, the device displayed obviously suppressed photocurrent hysteresis and achieved improved device PCE (from 7.3% to 14.9%). Thereafter, Xu et al. demonstrated the underlying reason for the released hysteresis and enhanced passivation of PCBM in perovskite devices [61]. They found that PCBM can react with perovskite by forming the strong fullerene cage-iodide interaction to passivate the Pb-I antisite defects and reduce the anion migration within perovskite film, thus leading to hysteresis-free and highly efficient devices. Based on these results, Echegoyen et al. synthesized and applied a fullerene derivative with a long alkyl chain, [6,6]-phenyl-C_{61}-butyric acid 2-ethylhexyl ester (PCBEH) with enhanced solubility, as an ETL in inverted architecture devices [62]. The better solubility facilitated fullerene molecules to permeate more efficiently along grain boundaries of the perovskite layer and significantly enhanced the passivation effect and device performance. In order to further passivate bulk traps, fullerene materials were also used incorporated into perovskite layer as additives. Chiang et al. doped 0.1 wt.% PCBM into PbI_2 precursor solution to form the mixed phase of PCBM/PbI_2, then the methylammonium iodide (MAI) solution reacted with the mixed PbI_2/PCBM film to form the pin-hole free perovskite film [63]. This strategy efficiently reduced the defect density of perovskite film, and the corresponding device yielded an increased PCE of 16.0% with a high FF of 0.82. Furthermore, Wu et al. creatively constructed a graded heterojunction (GHJ) structured perovskite film with PCBM and obtained a remarkable certified PCE of 18.12% based on a large active area (1.022 cm^2) [64]. In this GHJ structure, PCBM passivated the interfacial defects between perovskite and ETL, shortened the diffusion pathway of electrons through the perovskite film, and promoted the charge carriers' transfer and collection, leading to improved device performance. In addition, a bis-adduct fullerene derivative, α-bis-PCBM, was also used to regulate the growth of perovskite films and passivate the surface defects, thereby improving device performance [65].

Furthermore, fullerene materials were also applied to reduce the interface trap states between the IETL and perovskite layer. For example, Li et al. synthesized a new fullerene derivative, [6,6]-phenyl-C_{61}-butyric acid-dioctyl-3,3-(5-hydroxy-1,3-phenylene)-bis(2-cyanoacrylate) ester (PCBB-2CN-2C8), to modify the perovskite/TiO_2 surface [66]. Because the PCBB-2CN-2C8 can efficiently passivate the interface defects of perovskite/TiO_2 and improve the capacity of charge extraction of TiO_2, they finally obtained an improved PCE of 20.7%. PCBM also can passivate the defects of the aluminum-doped ZnO (AZO) layer to enhance the interfacial charge transfer and suppress the photocurrent hysteresis [67]. Therefore, as a kind of effective passivation reagent, fullerene materials should receive more attention and exploration.

2.3 Fullerenes as encapsulation layers in PSCs

The device stability is essential to its commercial application. As we know, perovskite materials are very sensitive to environmental conditions, such as moisture, oxygen, and ultraviolet (UV) light in ambient, which can lead to degradation of the perovskite layer and invalidation of the PSCs. Meanwhile, the surface and grain boundary defects in perovskite film would induce ion migration, leading to accelerated degradation of the perovskite film. Therefore, finding strategies to prevent this degradation is key to improving device stability. The fullerene materials with functions of suppressing ions diffusion and encapsulation can provide effective protection for perovskite film and device [68]. As reported in Refs. [61, 69], C_{60} and PCBM can react with perovskite by forming the strong fullerene cage-iodide chemical interaction. This interaction can suppress the anion migration within perovskite film efficiently, leading to improved device stability. Furthermore, besides the chemical interaction of the fullerene cage-iodine can inhibit ion migration, some special functional groups modified on the fullerene cage can also interact with perovskite to inhibit ion migration and increase device stability. Kan et al. synthesized a polyethylene glycol-modified fullerene (PCBHGE) and incorporated it into the perovskite films [47]. The functional group of PCBHGE can interact with the $[PbI_6]^{4-}$ octahedra by forming Lewis acid-base pairs, which substantially suppressed the ion migration in perovskite films. Thereby, the corresponding devices exhibited good stability that retains 87% of their initial value after storing in the dark for 203 days. Similarly, Huang et al. found that fluorinated fullerenes can interact with perovskite films by forming the hydrogen bonds between 5F-PCBP and MA^+ cations to immobilize these cations [70]. As a result, the strong H-bond completely hindered the undesired component migration, improving device stability to a T_{80} lifetime of reaching 1,920 h.

Functional fullerene materials were also used as encapsulation layers to address the device stability issues [71–74]. As shown in Fig. 2(g), Bai et al. developed a cross-linkable fullerene via the chemical interactions between fullerene molecules and incorporated it into PSCs as an encapsulation layer [53]. The hydrogen bonds between the carboxyl group (–COOH) of a self-assembled fullerene monolayer (C_{60}-SAM) and the hydroxyl (–OH) of silane can realize the cross-linked C_{60}-SAM layer with strong hydrophobicity (Fig. 2(h)). In contrast with the non-crosslinked C_{60}-SAM layer, the cross-linked one exhibited a larger water contact angle (86° vs. 46°, Fig. 2(i)), indicating great water resistance characteristics. This cross-linked C_{60}-SAM film can play the role of ETLs and the protective layer for the perovskite film. The device achieved outstanding moisture stability, retaining 90% of its initial PCE after exposure to ambient air. Specifically, the flexible side chains of functionalized fullerenes can also fill the cavities between the fullerene spheres to form a dense fullerene film or permeate into the grain boundaries of the perovskite layer to block the immersion of moisture and oxygen, thus improving the device stability [62, 75]. Therefore, fullerene materials with specific functional groups can play an important role in protecting perovskite films and improving the stability of corresponding devices.

3 Fullerene-related chemical interactions in PSCs

Fullerene-related chemical interactions in PSCs can be divided into fullerene-perovskite, fullerene-IETL, and fullerene-fullerene. Understanding how the fullerene-related chemical interactions impact the device performance is a favor to design novel functional fullerene materials for high-performance PSCs.

3.1 Chemical interaction of fullerene-perovskite

The solution-processed perovskite films contain a large number of grain boundary defects, which not only affect the PCE of devices but also cause serious device stability problems. Many previous works have proved that the functional groups (such as ester, oligoether, amine, heterocyclic pyridine, heterocyclic thiophene, porphyrin, and halogens) of fullerene materials can form chemical interactions (such as coordination bonds or hydrogen bonds) with perovskites [76]. These interactions effectively enhanced the passivation effect of fullerene on the defects of the perovskite films and improved the stability of the devices.

The ester group of fullerene materials can coordinate with the exposed interface lead ions of perovskite film, resulting in reduced non-radiative recombination. Echegoyen and co-workers also demonstrated the mechanism of the interactions between fullerene and perovskite using the density functional theory (DFT) [77]. As shown in Fig. 3(a), the carbonyl oxygen atoms of PCBM molecules located at the (110) surface of perovskite film can strongly associate with the lead atoms of perovskite film to form a dense and ordered PCBM layer. This interaction makes the ester group of PCBM closer to the perovskite than the fullerene carbon cage [78]. It also found that the ester groups of PCBM molecules deposited on the (100) surface of the perovskite film can generate hydrogen bonds between the carbonyl oxygen atoms of PCBM and the H atoms on the surface of the perovskite film (Fig. 3(b)). These two interactions between PCBM and perovskite vastly accelerate the electron extraction in the corresponding devices.

The existence of this interaction is also verified through experiments. Xie et al. introduced the hexakis [di(ethoxycarbonyl)methano]-C_{60} (HEMC) into perovskites with different components [79]. As shown in Fig. 3(c), HEMC with twelve ester groups can interact with unsaturated Pb^{2+} to form a trap-free perovskite film via the formed bonds between C=O bonds and Pb^{2+} ions. This can be observed from the Fourier transform infrared (FTIR) results (Fig. 3(d)) that the signal of C=O vibration of HEMC-PbI_2 showed a slight shift to the low wavenumber from 1,745 to 1,740 cm^{-1}, suggesting the interaction of fullerene and perovskite. Finally, they obtained a high PCE of over 20% with outstanding stability in storage, thermal, and light-soaking. Similarly, we designed several fulleropyrrolidine derivatives (2,5-(dimethyl ester) C_{60} fulleropyrrolidine ($DMEC_{60}$), 2,5-(dimethyl ester) C_{70} fulleropyrrolidine ($DMEC_{70}$), and bis-$DMEC_{60}$) and incorporated them into PSCs (Fig. 3(e)) [80, 81]. We found that the ester groups in these fullerenes can coordinate with the lead in perovskite films, thereby improving the PCE and yielding impressive device stability. Meanwhile, we also applied a new dimeric fullerene derivative, D-C_{60}, as ETL for fabricating inverted PSCs [82]. Benefiting from the hydrophobic surface of D-C_{60}, we achieved a device PCE of 16.6% with improved device stability.

As shown in Fig. 3(f), 2,5-diphenyl C_{60} fulleropyrrolidine (DPC_{60}) with a cis-configuration amine functional groups onto the C_{60} cage is also beneficial to form the interaction between DPC_{60} and perovskite [83]. As confirmed by X-ray photoelectron spectroscopy (XPS) measurements (Fig. 3(g)), the I 3d signal of PbI_2 has a slight shift towards higher bind energy after treating with DPC_{60}, indicating the formation of chemical interaction between PbI_2 and DPC_{60}. This interaction effectively elevated the passivation effect of the defects in the perovskite films. Finally, the fabricated PSCs with a structure of SnO_2/DPC_{60}/perovskite yielded a high PCE of 20.4%. Besides, the N atoms of pyridine and S atoms of thiophene also coordinate easily with the Pb^{2+} ions due to the donating electrons ability of N and S atoms [84]. As shown in Fig. 3(h), pyridine-functionalized fullerene derivative, [6,6]-(4-pyridinyl)-C_{61}-ethyl acid ethyl ester (PyCEE), was synthesized and proposed to construct the chemical interaction with the perovskite

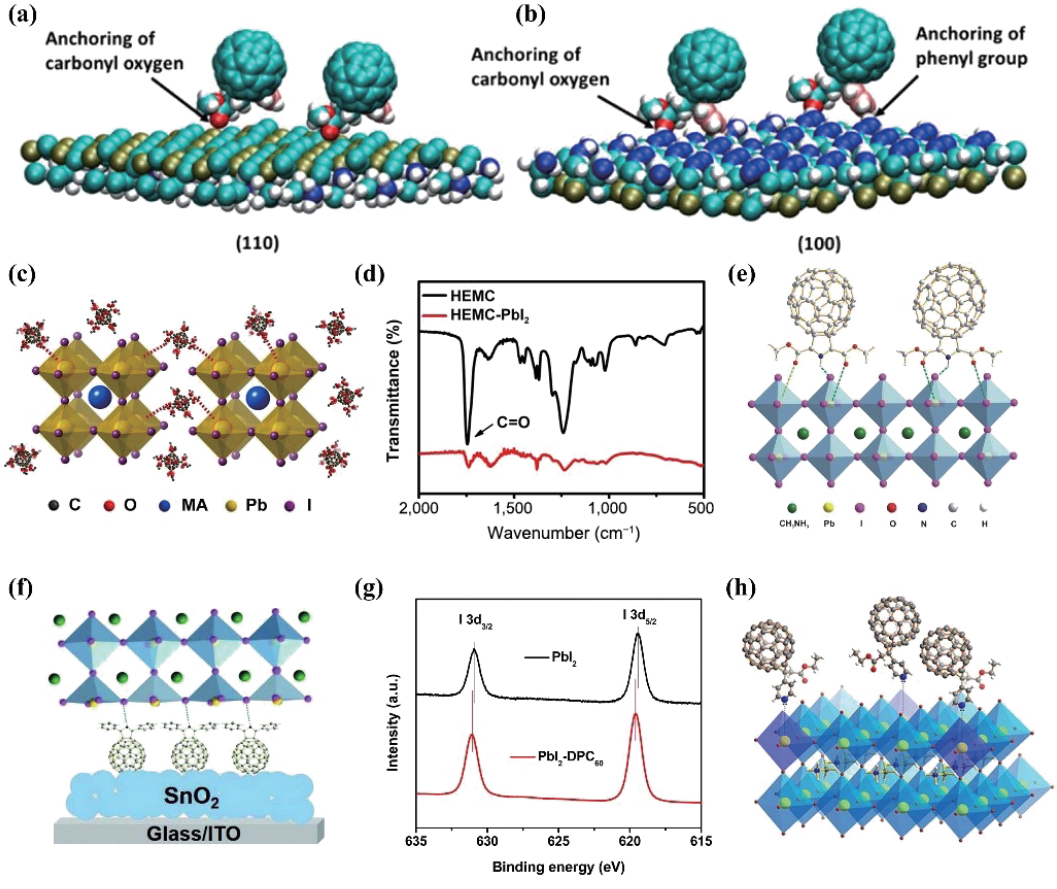

Figure 3 Schematic illustration of PCBM molecules attaching to the (a) (110) surface and (b) (100) surface of the perovskite film. Reproduced with permission from Ref. [78], © American Chemical Society 2016. (c) Illustration of the HEMC-based PSCs (the red dotted lines show the interaction between the HEMC and perovskite). (d) FTIR spectra of HEMC and HEMC-PbI_2. Reproduced with permission from Ref. [79], © Elsevier Ltd. 2020. (e) Schematic diagram of the interactions between fullerenes ($DMEC_{60}$ and $DMEC_{70}$) and perovskite film. Reproduced with permission from Ref. [80], © American Chemical Society 2016. (f) Schematic view of the interfacial modification showing a bonding effect between DPC_{60} and perovskite (green dashed lines). (g) XPS curves of the I 3d level for the PbI_2 and DPC_{60}-PbI_2 films. Reproduced with permission from Ref. [83], © WILEY-VCH Verlag GmbH & Co. KGaA, Weinheim 2019. (h) Schematic illustration of the interaction between PyCEE and perovskite. Reproduced with permission from Ref. [85], © American Chemical Society 2019.

layer [85]. The N atoms of the pyridine moiety of PyCEE can donate electrons to the Pb^{2+} ions to form the coordination bond. Thanks to this coordination, the PyCEE based ETL displayed obviously improved efficiency of the charge transfer at the interface of perovskite/PyCEE. Li et al. also verified that the chemical interactions between the N atoms of pyridine moiety and the Pb atoms of perovskite film could passivate the defects within perovskite film by reducing the non-radiative recombination [86, 87].

As shown in Fig. 4(a), Wang et al. inserted a new fullerene derivative, [6,6]-phenyl-C_{61}-butyric acid-N,N-dimethyl-3-(2-thienyl)propanam ester (PCBB-S-N), between perovskite film and PCBM layer as an interlayer to heal the interfacial defects [42]. The S atoms of thiophene in PCBB-S-N can bond with the under-coordinated lead ions to passivate the traps in perovskite film (Fig. 4(b)). Meanwhile, the amino moiety can form hydrogen bonds to prevent moisture from permeating into perovskite film. Furthermore, benefitting from the well-matched energy level alignment, decreased energy barrier, and enhanced charge transfer, the PCBB-S-N based device achieved a PCE of 21.08%.

Fullerene derivatives with halogen-containing functional groups into PSCs as additives, ETLs, or interfacial layers also exhibited a positive role in assisting the growth of perovskite film, reducing photocurrent hysteresis and improving the device stability [88, 89]. Wang et al. incorporated the novel fulleropyrrolidine (NMBF-Cl and NMBF-H) as interlayers at the interface of perovskite/SnO_2 [90], which can react between the Cl atoms of NMBF-Cl and the Pb atom of perovskite (Fig. 4(c)). Meanwhile, the shift in binding energy of perovskite film with NMBF-Cl treatment indicated the formed interaction between NMBF-Cl and perovskite (Fig. 4(d)). As a result, a decent PCE of 22.3% was obtained for the NMBF-Cl based PSCs. Fullerene derivative containing the iodide quaternized tri(dimethylamine), PCBB-3N-3I, can also efficiently passivate the defects of perovskite film [91]. The I^- of PCBB-3N-3I can coordinate with the Pb^{2+} of perovskite film via electrostatic interaction to passivate the positively charged defects in perovskite film.

At the same time, the fluorinated fullerenes have also received more attention [92–94]. Rajagopal et al. incorporated the fluoroalkyl-substituted fullerene (DF-C_{60}) into the Pb-Sn

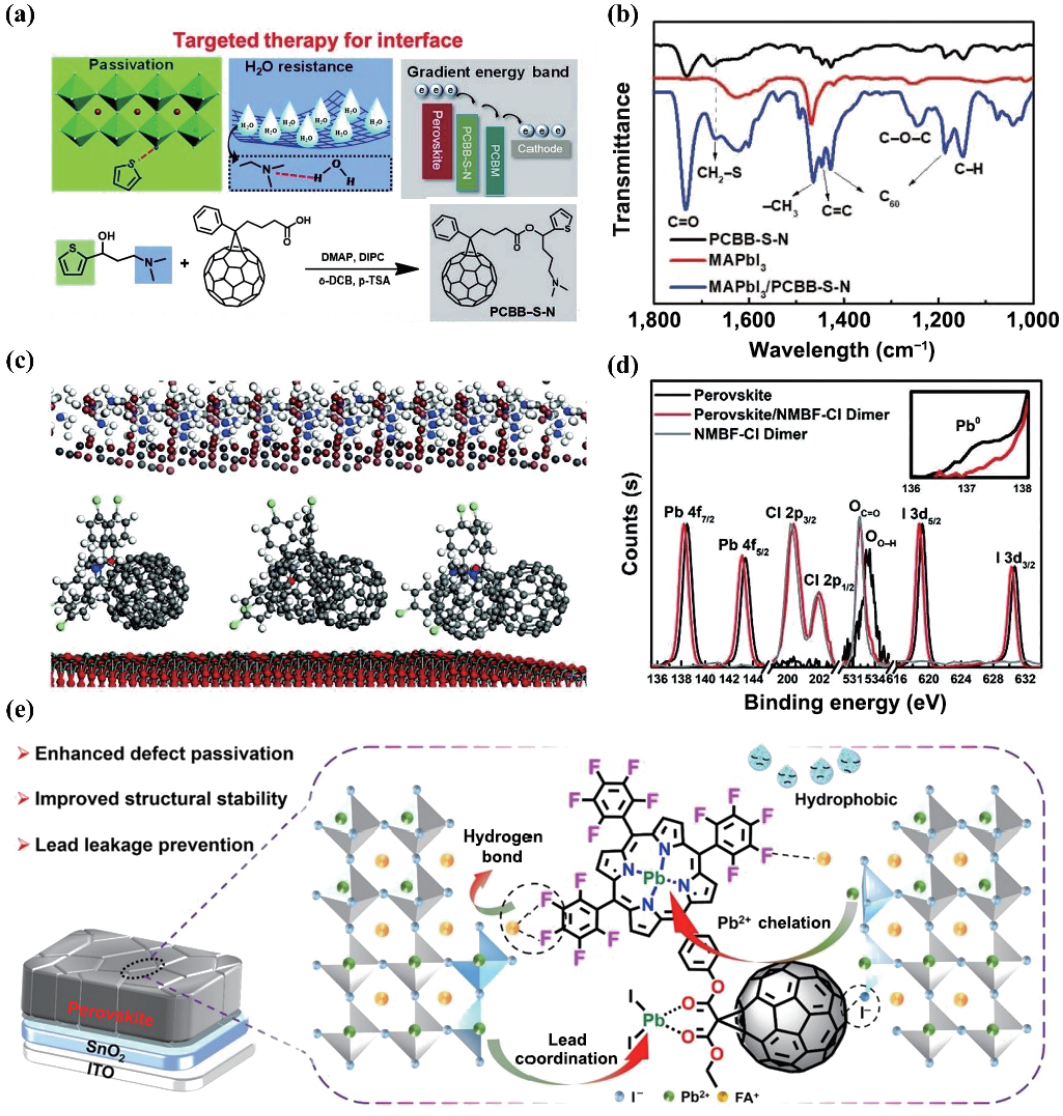

Figure 4 (a) The role of PCBB-S-N as an intermediary layer in devices: passivation of defects, H_2O resistance, and the formation of gradient energy band (top). The synthetic route and chemical structure of the PCBB-S-N molecules (bottom). (b) FTIR spectra of the pristine $MAPbI_3$ film, PCBB-S-N film, and $MAPbI_3$/PCBB-S-N film. Reproduced with permission from Ref. [42], © WILEY-VCH Verlag GmbH & Co. KGaA, Weinheim 2019. (c) Simulated interactions at the perovskite/SnO_2 interfaces with the presence of NMBF-Cl dimer at the interface (the simulations employ SnO_2 (110) surfaces with Sn and O terminals and $MAPbI_3$ (110) surfaces with Pb and I terminals). (d) XPS spectra of pristine perovskite film, NMBF-Cl dimer film and perovskite/fullerene film. Reproduced with permission from Ref. [90], © WILEY-VCH Verlag GmbH & Co. KGaA, Weinheim 2020. (e) Schematic view of the FPD-assisted lead leakage prevention and performance improvement strategy for PSCs. Reproduced with permission from Ref. [45], © WILEY-VCH 2021.

perovskite film, forming the graded heterojunction structure, and passivating the defects in perovskite film via the formed hydrogen bond [95]. Chang et al. introduced the fluorinated fullerene into perovskite film, where the 3F-$PC_{61}BM$ can assist the growth process of perovskite grains to form a dense and defect-less perovskite film [96].

Recently, the chemical interactions between porphyrin-functionalized fullerene and perovskite were also applied to enhance device performance and prevent the lead leakage. As shown in Fig. 4(e), we designed a functional fullerene, fullerene-porphyrin dyad (FPD), composed of a C_{60} cage, a porphyrin ring, and three pentafluorophenyl groups [45]. As confirmed by XPS spectra, ^{19}F nuclear magnetic resonance (NMR) spectra and FTIR spectra, several different types of chemical interactions, including hydrogen bond, lead coordination, and electrostatic interaction, were formed between FPD and perovskite. The above interactions effectively enhance the FPD's defect passivation capability and structural stability under continuous irradiation. As a result, we present a superior PCE of 23% and remarkably improved operational stability, retaining > 83% of its initial efficiency after 1,500 h of maximum power point tracking under one sun continuous irradiation. Moreover, the porphyrin ring could react with lead ions to form a water-insoluble and stable FPD-Pb complex, thus reducing the risk of lead leakage. Meanwhile, FPD showed effective inhibition of the thermal decomposition of perovskite. The summary of the device parameters is shown in Table 1.

3.2 Chemical interactions of fullerene-IETL

Fullerene materials can change the surface electron structure of the underlying layers to regulate the energy level alignment. Figure 5(a) shows a fullerene derivative, carboxyl-functionalized carbon buckyballs, C_{60} pyrrolidine tris-acid (CPTA), was used to modify the indium-tin oxide (ITO) electrode [37]. The high electronegative carboxyl group of CPTA can be tightly anchored to the ITO surface by replacing the original hydroxyl groups. The interactions facilitated the CPTA molecules forming a robust film between the ITO and perovskite layer. Finally, benefiting from the tuned WF of ITO by CPTA and enhanced charge transfer, the corresponding devices yielded PCEs of 18.39% and 17.04% on the rigid and flexible substrates, respectively. Especially, the CPTA-based flexible device remained 93% of its initial PCE without hysteresis after bending for 1,000 cycles (Fig. 5(b)).

Fullerene materials also can be used to modify the metal oxide film like TiO_2 and SnO_2 to enhance the charge transfer by tuning the energy level or passivating the surface defects. In 2013, Abrusci et al. introduced a C_{60}SAM to modify the underlying mesoporous TiO_2 (Fig. 5(c)) [97]. The matched energy level alignment between C_{60}SAM and perovskite film promoted the thermal electrons transferring freely back and forth between these two function layers. Compared with the original perovskite film, C_{60}SAM-based perovskite film displayed a faster PL decay, suggesting the fast and efficient electrons transport associated with the C_{60}SAM (Fig. 5(d)). Benefiting from the above advantages, the device with C_{60}SAM exhibited a notable increased PCE of 6.7% with a significantly improved FF and a slightly improved V_{OC}. Similarly, the carboxyl group of [6,6]-phenyl-C_{61} butyric acid (PCBA) can interact with TiO_2 to reduce the traps sites in TiO_2 film and suppress the charge recombination at the TiO_2/perovskite interface [98]. In addition, fullerenes with halide groups can also through the strong interaction passivate the defects in TiO_2 and reduce the hysteresis effect induced by the trap-mediated recombination [99].

Many works have reported the potential ability of fullerene materials in eliminating the traps within SnO_2 film [100, 101]. Wang et al. applied C_{60}, PCBM, and PCBA to modify the SnO_2 ETL and gained a PCE of 18.8% for the device with the PCBA-modified SnO_2 ETL [102]. Verified by ultraviolet photoelectron spectroscopy (UPS) analysis, PCBA improves the work function of SnO_2 from 3.58 to 4.00 eV, which helps to form a surface dipole, inducing an increase of the electric field and promoting the charge collection. Liu et al. employed a fullerene derivative, 9-(1-(6-(3,5-bis(hydroxymethyl)phenoxy)-1-hexyl)-1H-1,2,3-triazol-4-yl)-1-nonyl [60] fullerenoacetate (C9), to anchor on the SnO_2 surface to passivate the surface traps of SnO_2 films [103]. As shown in Fig. 5(e), the hydroxyl terminal of C9 can provide extra electrons to fill the oxygen vacancies and interact with the uncoordinated Sn in SnO_2. These interactions reduced the traps, enhanced the extraction of photo-generated charge carriers, and suppressed the traps-related recombination. Meanwhile, the strong hydrophobicity of SnO_2/C9 film suppressed the heterogeneous nucleation when depositing perovskite solution on SnO_2/C9 film, which is beneficial to grow a smooth perovskite film with large crystal grains. Finally, the C9-based device showed an improved PCE of 21.3%. Similarly, Cao et al. inserted a fullerene derivative,

Table 1 Device performance summaries of PSCs containing functionalized fullerene and perovskite materials

Device structure	V_{OC} (V)	J_{SC} (mA·cm^{-2})	FF (%)	PCE (%)	References
FTO/NiO_x/perovskite (HEMC)/HEMC/PCBM/BCP/Ag	1.10	22.84	80.58	20.02	[79]
FTO/PEDOT:PSS/perovskite/DMC_{60}/LiF/Al	0.92	21.73	75.80	15.20	[80]
FTO/PEDOT:PSS/perovskite/DMC_{70}/LiF/Al	0.95	22.44	77.10	16.40	[80]
ITO/SnO_2/DPC_{60}/perovskite/Spiro-OMeTAD/Au	1.14	23.01	77.72	20.35	[83]
FTO/PyCEE/perovskite/Spiro-OMeTAD/Ag	1.05	22.95	75.83	18.27	[85]
ITO/NiO_x/perovskite/PC_{61}Bpy/BCP/Ag	0.96	24.85	75.0	17.84	[77]
FTO/TiO_2/ZrO_2/carbon-perovskite (bis-$DMEC_{60}$)	0.92	23.30	71.02	15.21	[81]
ITO/PEDOT:PSS/perovskite/PC_{61}BM/D-C_{60}/Au	0.96	21.89	78.8	16.6	[82]
ITO/PTAA/perovskite/PCBB-S-N/PCBM/Al	1.12	23.82	79.09	21.08	[42]
ITO/SnO_2/perovskite-FPD/Spiro-OMeTAD/Ag	1.13	25.19	80.86	23.00	[45]
ITO/SnO_2/NMBF-Cl/perovskite/Spiro-OMeTAD/Ag	1.12	25.7	77.1	22.3	[90]
ITO/PTAA/perovskite/PCBB-3N-3I/PCBM/Al	1.15	23.46	81.36	21.10	[91]
ITO/PEDOT:PSS/perovskite:DF-C_{60}/IC_{60}BA/bis-C_{60}/Ag	0.87	26.1	0.69	15.61	[95]
ITO/PEDOT:PSS/perovskite:3F-PC_{61}BM/PCBM/PEI/Au	1.00	21.78	73.34	16.17	[96]
ITO/PTAA/perovskite/PCBBOEG/PCBM/Al	1.07	23.65	80.0	20.2	[104]

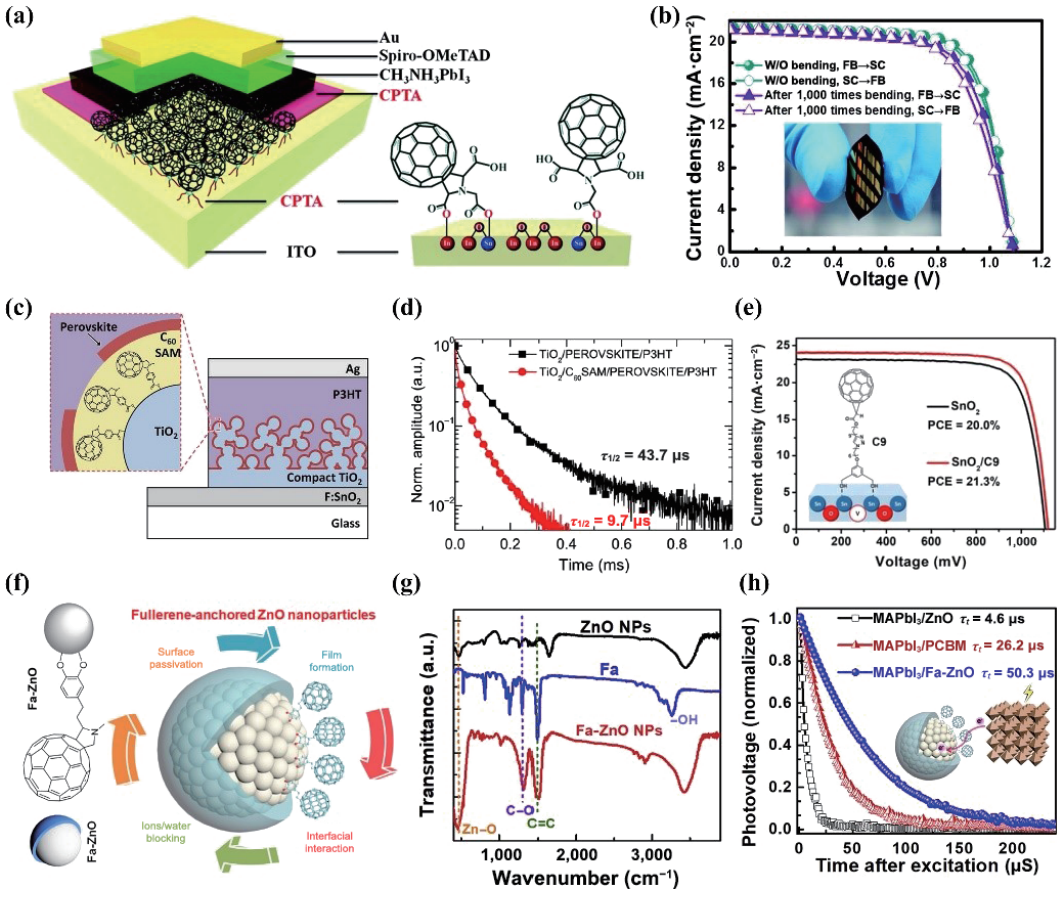

Figure 5 (a) Schematic diagram of the interaction between CPTA and ITO, and the corresponding device structure. (b) The reverse and forward current density–voltage (*J*–*V*) scans curves of the flexible device before and after 1,000 bending cycles with the device structure of PET/ITO/CPTA/$CH_3NH_3PbI_3$/Spiro-OMeTAD/Au (the inset shows a photograph of the CPTA-based flexible PSC). Reproduced with permission from Ref. [37], © WILEY-VCH Verlag GmbH & Co. KGaA, Weinheim 2017. (c) Schematic of the insertion of C_{60}SAM between perovskite and TiO_2 in the n–i–p structure device. (d) Transient photocurrent decays trace for two devices with and without C_{60}SAM. Reproduced with permission from Ref. [97], © American Chemical Society 2013. (e) The *J*–*V* curves of the device without and with C9 as an interfacial layer. The inset demonstrates the schematic of the interaction between hydroxyl terminal of C9 and Sn of SnO_2. Reproduced with permission from Ref. [103], © The Royal Society of Chemistry 2018. (f) Chemical structure of the fullerene derivatives Fa (left side) and the schematic drawing of Fa coated ZnO NPs with core-shell structure (right side). (g) The FTIR spectra of ZnO, Fa, and Fa-ZnO. (h) Normalized TPV decay curves of $MAPbI_3$ films covered by various ETLs under white bias light of 1 sun (100 mW·cm^{-2}). The inset shows the process of charge transport. Reproduced with permission from Ref. [105], © Elsevier Inc. 2018.

pyrrolidinofullerene C_{60}-substituted phenol (NPC_{60}-OH), between SnO_2 and perovskite layer to form a SnO_2/NPC_{60}-OH structure. Due to the higher electron mobility of the SnO_2/NPC_{60}-OH and the enlarged grains of perovskite film, their devices yielded a higher PCE of 21.39% [39].

Fullerene materials can also be used to modify ZnO ETLs. As shown in Figs. 5(f) and 5(g), Yao et al. used a fullerene with catechol groups to anchor on the surface of ZnO nanoparticles (NPs) to form a core–shell structure via the interfacial interactions (Fa-ZnO) [105]. The resulting Fa-ZnO has fewer defects with enhanced capability to block ions diffusion and water penetration. Compared with the device without fullerene modification (Fig. 5(h)), the Fa-ZnO based device showed an improved recombination lifetime (50.3 μs vs. 4.6 μs), suggesting the effective passivation effect to the traps within Fa-ZnO film. As a result, the Fa-ZnO based device yielded an improved PCE of 21.1% with enhanced device stability. From the above discussions, we can conclude that the enhanced chemical interaction of fullerene-IETL can efficiently improve the device efficiency and stability [106, 107]. The device parameters that existing chemical interactions of fullerene-IETL are summarized in Table 2.

3.3 Chemical interactions of fullerene–fullerene

Fullerene-based films are prone to aggregate under light, high temperature, and solvent treatment conditions. These unexpected phenomena would lead to the performance loss of the fullerene-based device. The stable, robust, and dense fullerene films can play an effective protective layer to hinder the permeation of water and oxygen in ambient when applied in inverted structure PSCs and can also resist the solution of the subsequent solvent process when used in the normal structure PSCs. Thus, it is very important to find strategies to solve the stability issue of these fullerene films.

3.3.1 *Secondary bond linked fullerene molecules*

To enhance the stability of the fullerene-based film, a thermally stable fullerene ETL was developed by mixing the fullerene derivatives PCBM and [6,6]-phenyl-C_{61}-propylbenzene (PCPB) [108]. As shown in Fig. 6(a), PCBM and PCPB have a similar molecular structure and crystal packing. By tuning the weight ratios of PCBM and PCPB, the crystal showed "PCBM–PCPB–PCBM–PCPB" arrangement structure via the non-covalent intermolecular interactions. The intermolecular interactions between PCBM and PCPB can effectively suppress the diffusion and aggregation of them to keep a mixed phase, improving the morphological stability of the hybrid ETL. As a result, the device with this hybrid ETL exhibited good thermal stability that retained 80% of its initial PCE under annealing at 85 °C in N_2 for 500 h, while the control device only retained 50% of initial PCE under the same condition (Fig. 6(b)). Similarly, Xing et al. mixed $PC_{61}BM$ with its derivatives with different lengths of

Table 2 The summary of device parameters of PSCs existing chemical interactions of fullerene-IETL

Device structure	V_{OC} (V)	J_{SC} (mA·cm^{-2})	FF (%)	PCE (%)	References
Glass/ITO/CPTA/perovskite/Spiro-OMeTAD/Au	1.10	22.06	75.61	18.39	[37]
PET/ITO/CPTA/perovskite/Spiro-OMeTAD/Au	1.09	21.35	73.13	17.04	[37]
Glass/FTO/TiO_2/PCBA/perovskite/Spiro-OMeTAD/Ag	1.16	21.38	72.0	17.76	[98]
Glass/FTO/TiO_2/NAMF-Cl/perovskite/Spiro-OMeTAD/Ag	1.08	22.7	78.60	19.3	[99]
PEN/ITO/SnO_2/CPTA/perovskite/Spiro-OMeTAD/Au	1.08	22.39	75.0	18.36	[100]
Glass/FTO/SnO_2/CPTA/perovskite/PTAA/Au	0.69	16.45	65.0	7.40	[101]
ITO/SnO_2/PCBA/perovskite/Spiro-OMeTAD/MoO_3/Au	1.10	22.2	76.0	18.6	[102]
Glass/ITO/SnO_2/C9/perovskite/Spiro-OMeTAD/Au	1.12	24.1	78.9	21.3	[103]
Glass/FTO/Cu:NiO_x/perovskite/Fa-ZnO/Ag	1.14	22.83	81.0	21.11	[105]
Glass/FTO/TiO_2/C_{60}SAM/perovskite/P3HT/Ag	0.8	—	—	6.7	[97]
Glass/ITO/Sol-gel ZnO/PCBM/perovskite/PTB7-Th/MoO_3/Ag	1.03	14.96	75.0	11.04	[107]

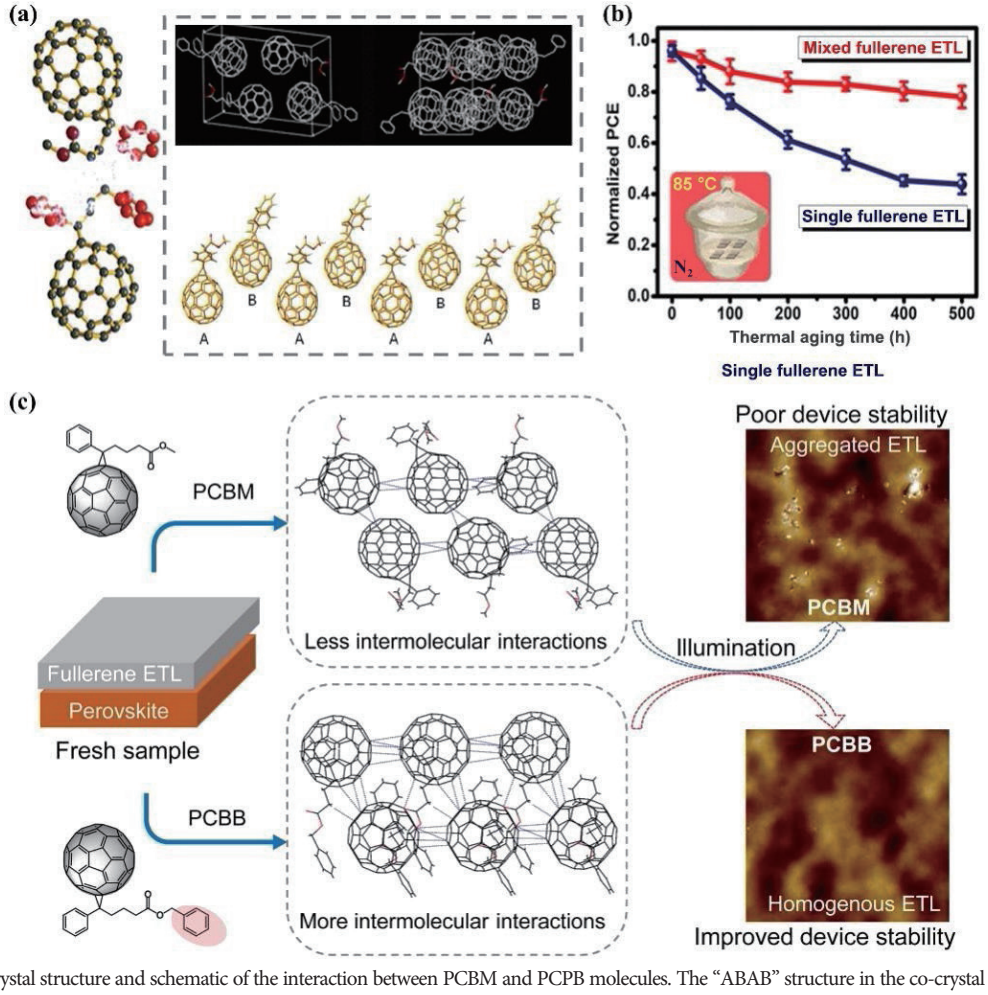

Figure 6 (a) The crystal structure and schematic of the interaction between PCBM and PCPB molecules. The "ABAB" structure in the co-crystal of PCBM and PCPB (upper right) and the cocrystal packing structure viewed along the *c* axis for the unit cell of PCPB and PCBM cocrystals (low right). (b) Thermal stability of PSCs after thermal ageing (85 °C) under an N_2 atmosphere. Reproduced with permission from Ref. [108], © American Chemical Society 2020. (c) Schematic illustration of the influence of fullerene's intermolecular interaction on device stability and atomic force microscopy images of the PCBM and PCBB films on the perovskite substrates, which were aged under continuous illumination without cooling (surface temperature: 55 °C; scale bar: 1 μm). Reproduced with permission from Ref. [110], © Science China Press 2020.

fluorocarbon chains, CF_3-$PC_{61}BM$ and C_3F_{13}-$PC_{61}BM$, to construct the blend fullerene ETL film with excellent water-resistant [109]. The fluorocarbon chains in CF_3-$PC_{61}BM$ and C_3F_{13}-$PC_{61}BM$ with improved hydrophobic property efficiently prevented the moisture from penetrating the ETLs and destroying the underlying perovskite film. More importantly, these devices with these ETLs exhibited good humidity stability, especially for the C_3F_{13}-$PC_{61}BM$-based PSCs demonstrated a T_{80} of 33 days under the storage condition of relative humidity (RH) 40%–60% without encapsulation.

Recently, we introduced a fullerene derivative, [6,6]-phenyl-C_{61}-butyric acid benzyl ester (PCBB), to replace the commonly used PCBM ETL in the inverted PSCs [110]. As shown in Fig. 6(c), PCBB has one more extra phenyl group than the PCBM, showing stronger intermolecular interactions. Expect for the intermolecular interactions between the C_{60} cages via the π–π interactions, the

extra phenyl group provided more intermolecular interactions between the functional groups via the CH–π interactions. These interactions efficiently suppressed the aggregation of PCBB induced by illumination. Compared with the PCBM-based device (retaining of 70% of its initial PCE), the PCBB-based device still maintained 90% of its initial PCE after working on the maximum power point condition under the continuous illumination over 600 h, exhibiting outstanding operational stability. Therefore, as mentioned above, the weak interaction in the fullerene film is important to construct a robust fullerene layer for PSCs. The summary of the related device parameters is shown in Table 3.

3.3.2 *Covalent bond linked fullerene molecules*

The covalent cross-linking is another strategy to suppress the aggregation and improve the film stability of the fullerenes, and it can also largely improve the mechanical stability of the flexible PSCs. For example, Wojciechowski et al. developed two cross-linkable fullerene derivatives, which are insolubilized in the aprotic solvents and used as ETLs in the regular n–i–p PSCs [111]. As shown in Fig. 7(a), the sol-gel C_{60}, containing a triethoxysilane moiety (N-[3-(triethoxysilyl) propyl]-2-carbOMethoxy-3,4-fulleropyrrolidine), realized the cross-linking via the formed Si–O–Si bonds when exposing to the trifluoroacetic acid (TFA) vapor. The other is phenyl-C_{61}-butyric acid benzocyclobutene ester (PCBCB) containing a benzocyclobutene group, which can be cross-linked via the thermal activation of the benzecyclobutene moiety at 200 °C for 10 min. These two fullerene films have high uniformity and well-controlled thickness. In addition, these two fullerene films showed no difference before and after washing with neat N'N-Dimethylformamide (DMF) and chlorobenzen (CB), exhibiting good stability and solvent resistance (Fig. 7(b)).

Other groups have demonstrated that cross-linking strategies can effectively improve the stability and practicability of fullerene films. For example, a fullerene derivative, [6,6]-phenyl-C_{61}-butyric styryl dendron ester (PCBSD), can be cross-linked with thermal cross-linker of the dendron containing two styryl groups [112]. The formed PCBSD film can efficiently passivate the trap states on the TiO_2 surface and tune the energy level alignment of adjacent layers. Similarly, Kang et al. reported a cross-linked fullerene, [6,6]-phenyl-C_{61}-butyric styryl dendron ester (C-PCBSD), which can be cross-linked under the thermal treatment at 160 °C [113]. Meanwhile, a similar cross-linkable fullerene, [6,6]-phenyl-C_{61}-butyric oxetane dendron ester (C-PCBOD), can be cross-linked without any cross-linking agent. These two cross-linked fullerene films can not only resist the solvent erosion in the sequent perovskite precursor solution, but also passivate the surface traps of TiO_2 film and regulate the energy level matching between TiO_2 and perovskite. Finally, the devices with C-PCBSD or C-PCBOD as an interfacial modifier on the TiO_2 film exhibited largely enhanced device performance.

The commonly used fullerene-based ETLs showed poor mechanical stability, which hindered their use in flexible devices. To address this issue, Watson et al. introduced a cross-linked fullerene (Fig. 7(c)), $MPMIC_{60}$, to replace the fragile fullerene-based ETLs such as C_{60} or $PC_{61}BM$ [114]. Compared with C_{60}- and $PC_{61}BM$-based devices, the device with a cross-linked $MPMIC_{60}$ film exhibited an obvious enhancement of fracture resistance. Moreover, the energy level of the cross-linked $MPMIC_{60}$ film matched well with perovskite film, exhibiting improved efficiency of electrons extraction. Thus, the cross-linked $MPMIC_{60}$ film simultaneously enhanced the device photovoltaic performance and mechanical stability. Afterward, Song et al. heated the C_{60} film at 150 °C for 60 s with a poly(allylamine) (PAA) as the cross-linked agent to obtain an insoluble C_{60}-PAA film [115]. As shown in Fig. 7(d), the amine groups of PAA can react with C_{60} molecules through nucleophilic under thermal treatment condition, forming a homogenous and robust C_{60}-PAA film, which showed good solvent resistance even washing with the mixed solvent of DMF and dimethyl sulfoxide (DMSO). Finally, the device retained 83% of the initial PCE after 600 bending cycles (Fig. 7(e)).

Lately, Li et al. reported that they incorporated the photo-crosslinked fullerene derivative, [6,6]-phenyl-C_{61}-butyric oxetane dendron ester (C-PCBOD), into the perovskite as the additive [116]. As shown in Fig. 7(f), the *in-situ* cross-linked C-PCBOD was realized by ring-opening polymerization under UV light irradiation. The C-PCBOD can insert into the annealed perovskite film along with the grain boundaries, forming an organic network to act as a plasticizer to increase the mechanical durability of perovskite film. Meanwhile, the cross-linked C-PCBOD effectively passivated the traps within the perovskite film. Therefore, the device with C-PCBOD exhibited an enhanced efficiency and displayed a decreased degradation in PCE even under the gradient increased stretching amount (Fig. 7(g)).

4 Summary and outlook of the fullerene in PSCs

Fullerenes and their derivatives have shown great advantages in the fabrication of inverted and normal PSCs. Fullerenes can be

Table 3 The summary of device parameters that existing interaction effect as well as cross-linked fullerenes in various fullerenes with different functional groups

Device structure	V_{OC} (V)	J_{SC} (mA·cm^{-2})	FF (%)	PCE (%)	References
FTO/NiO_x/perovskite/PCBM/PCPB/BCP/Ag	1.09	22.88	76.74	18.48	[108]
FTO/NiO_x/perovskite/CF_3-$PC_{61}BM$/BCP/Ag	1.06	22.61	76.97	18.37	[109]
FTO/NiO_x/perovskite/C_6F_{13}-$PC_{61}BM$/BCP/Ag	1.06	22.61	76.20	17.71	[109]
FTO/NiO_x/perovskite/PCBB/BCP/Ag	1.08	22.85	80.39	19.84	[110]
FTO/sol-gel C_{60}/perovskite/Spiro-oMeTAD/Au	1.07	23.0	73.0	17.9	[111]
FTO/PCBCB/perovskite/Spiro-oMeTAD/Au	1.11	22.4	73.0	17.9	[111]
FTO/TiO_2/PCBSD/perovskite/Spiro-oMeTAD/Au	1.12	21.1	79.0	18.7	[112]
ITO/TiO_2 (Au)/C-PCBSD/perovskite/Spiro-oMeTAD/Au	1.01	22.23	68.22	15.32	[113]
ITO/mp-TiO_2/C-PCBOD/perovskite/Spiro-oMeTAD/Au	1.04	23.99	73.25	18.29	[113]
ITO/$MPMIC_{60}$/perovskite/Spiro-oMeTAD/Ag	1.08	20.2	64.0	13.8	[114]
ITO/PEDOT:PSS/perovskite/$MPMIC_{60}$/ZnO/Al	0.81	19.0	78.0	12.3	[114]
FTO/TiO_2/C_{60}-PAA /perovskite/Spiro-oMeTAD/Ag	1.04	20.7	70.5	15.2	[115]
PET/ITO/TiO_x/perovskite-C-PCBOD/Spiro-oMeTAD/MoO_3/Ag	1.10	21.62	76.0	18.1	[116]

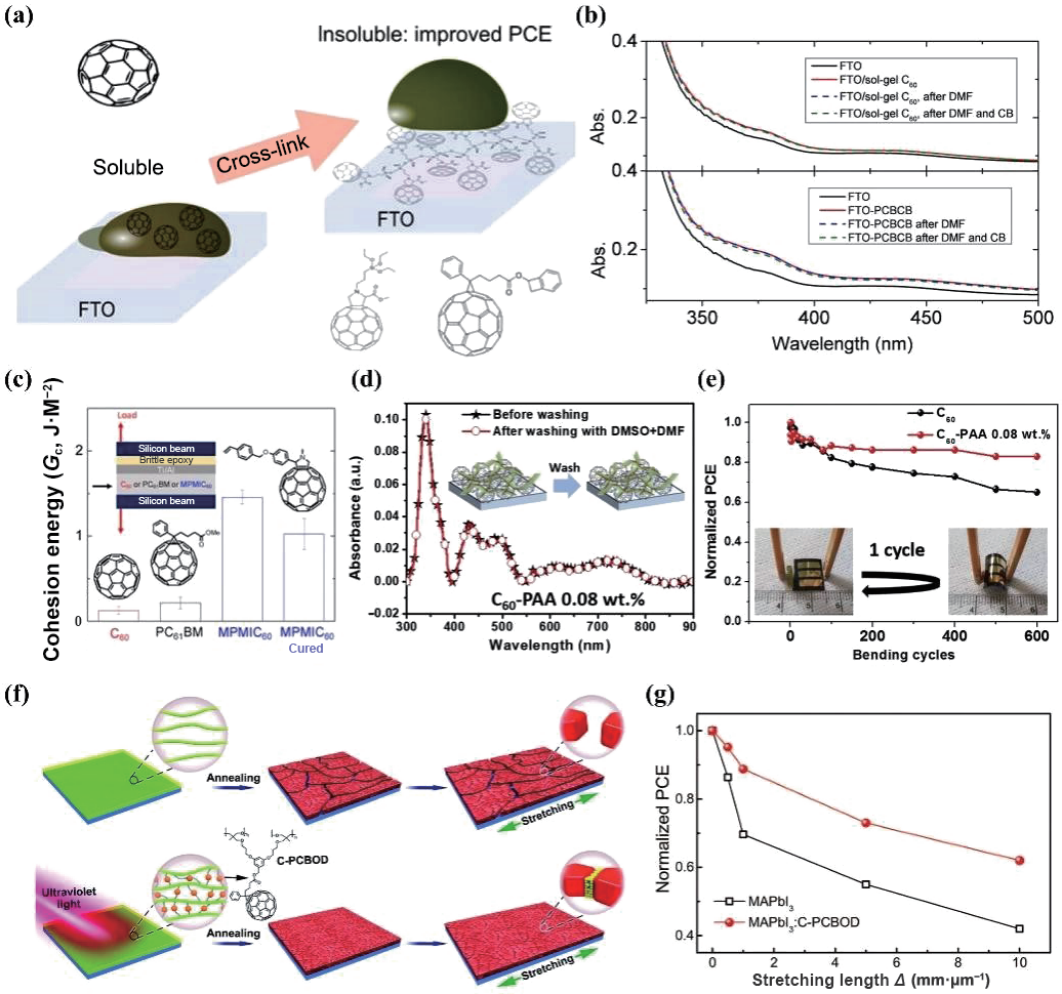

Figure 7 (a) Schematic diagram of the cross-linkable fullerene derivatives in improving the adhesion of fullerene layer on FTO substrate. (b) Effect of the neat solvents on cross-linked films. Reproduced with permission from Ref. [111], © American Chemical Society 2016. (c) The cohesion energy of C_{60}, $PC_{61}BM$, $MPMIC_{60}$ and the cured $MPMIC_{60}$. The inset showed the cured $MPMIC_{60}$ can enhance device fracture resistance. Reproduced with permission from Ref. [114], © American Chemical Society 2016. (d) Ultraviolet–visible (UV–Vis) absorption spectra of the PAA layers on FTO glass before (black line) and after washing with the mixed solvent of DMF and DMSO. (e) Normalized PCEs of the flexible devices employing C_{60} and C_{60}-PAA (0.08 wt.%) ETLs as a function of bending cycle (radius of bending = 10 mm). Reproduced with permission from Ref. [115], © Elsevier Ltd. 2018. (f) The formation of the cross-linked PCBOD-perovskite under illuminating with UV (254 nm) for 5 min for the wet perovskite film. After annealing, the C-PCBOD molecules fill the spaces between the grain boundaries forming an organic network around the perovskite grains; (g) the normalized PCE of $MAPbI_3$ flexible PSCs with and without C-PCBOD as a function of the stretching length. Reproduced with permission from Ref. [116], © WILEY-VCH Verlag GmbH & Co. KGaA, Weinheim 2019.

used as ETLs, passivator, and encapsulation layers to improve the device performance. Especially, the chemical interactions between fullerene molecules and between fullerene and adjacent layers are significantly crucial for the device performance. Enhancing the chemical interactions of fullerene-perovskite, fullerene-IETLs, and fullerene–fullerene can not only improve the device efficiency and suppress the hysteresis but also effectively improve the device stability.

Firstly, the chemical interaction of fullerene-perovskite can be realized by using fullerene derivatives with special functional groups as an interface modification material of the perovskite layer or using as additive incorporated into perovskite layers. These chemical interactions can effectively promote the passivation effect of fullerene on perovskite defects, inhibit the recombination of carriers, and reduce the hysteresis effect of the device. It should be noted that the released hysteresis of PSCs could be attributed to the fullerene-perovskite chemical interactions, which not only improve the passivation effect of the traps but also enhance the electron extraction. At the same time, this enhanced chemical interaction can also effectively suppress ion migration, improve device stability, and even prevent lead leakage of the PSCs. Secondly, the functional groups, including carboxyl group, hydroxyl group, and halides on fullerene cage, can anchor on the surface of ITO or IETLs such as ZnO, TiO_2, and SnO_2 to form fullerene-IETL interactions. These interactions can tune the WF and reduce the surface traps of the IETL, thereby promoting charge extraction and transfer. Meanwhile, the hydrophobic surface of fullerenes can prevent moisture from invading the device, which is beneficial to improve the device stability. Furthermore, it can suppress the heterogeneous nucleation to improve the quality of the upper perovskite film, thus yielding efficient PSCs. Lastly, the aggregation of fullerenes caused by light soaking, annealing treatment, and solvent atmosphere is another important issue, which may lead to decreased device performance. The fullerene film stability can be improved by increasing the secondary or covalent bond chemical interactions between fullerene molecules. The fullerene ETLs with enhanced interactions can not only be used for the inverted devices to protect the underlying perovskite film but also can be used for normal devices to improve the efficiency of the electron extraction. However, almost all the reported cross-linkable fullerene derivatives still require high temperatures to crosslink, which limits their compatibility in devices with a different structure. Meanwhile, the efficiency and stability of fullerene-based PSCs still

need to be improved. Therefore, further developing novel fullerene derivatives with specific functional groups to enhance the fullerene-related chemical interaction is highly desired.

Finally, we believe that designing the new functional fullerene materials with multiple functions is significantly important for improving the fullerene-related device performance as well as the further application of fullerene materials in more research fields. As shown in Fig. 8, the following suggestions are proposed to further facilitate the researches of fullerenes and fullerene-based PSCs: (1) design and synthesize special functional fullerene derivatives to enhance the related chemical interactions between fullerenes and adjacent function layers for passivating defects, suppressing the recombination of charge carriers, and preventing lead leakage; (2) design and synthesize some novel fullerene derivatives with high LUMO energy levels to realize the improvement in the V_{OC} of the wide-bandgap based perovskite and tin-based perovskite devices; (3) introduction of a functional group such as porphyrin in fullerene derivatives to facilitate their intramolecular electron transfer, thus increasing their electron mobility; (4) synthesis of low-temperature cross-linkable fullerene derivatives to improve the compatibility of cross-linkable fullerenes in various devices (the formal, inverted, tandem PSCs, etc.).

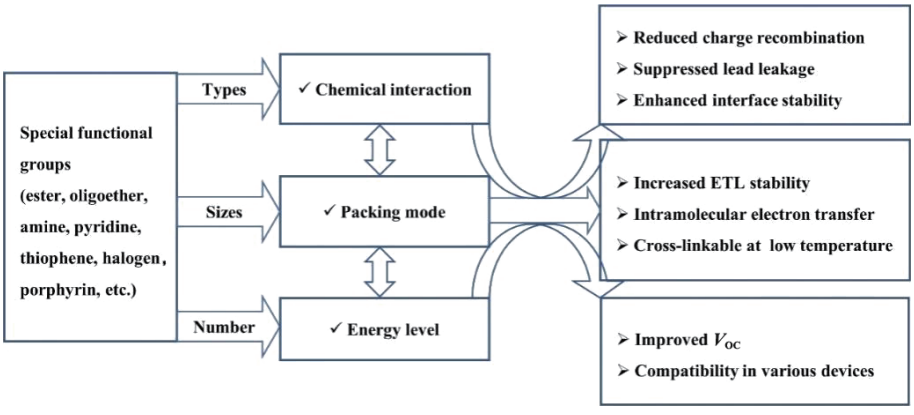

Figure 8 Promising strategies for developing fullerene materials.

Acknowledgements

This work was financially supported by the National Natural Science Foundation of China (Nos. 51902110, U21A2078, and 22179042), the Natural Science Foundation of Fujian Province (Nos. 2020J01064, 2020J06021, and 2019J01057), the Scientific Research Funds of Huaqiao University, and Promotion Program for Young and Middle-aged Teacher in Science and Technology Research of Huaqiao University (Nos. ZQN-806 and ZQN-PY607).

References

[1] Dresselhaus, M. S.; Crabtree, G. W.; Buchanan, M. V. Addressing grand energy challenges through advanced materials. *MRS Bull.* **2005**, *30*, 518–524.

[2] Liu, M. Z.; Johnston, M. B.; Snaith, H. J. Efficient planar heterojunction perovskite solar cells by vapour deposition. *Nature* **2013**, *501*, 395–398.

[3] Kim, H. S.; Lee, C. R.; Im, J. H.; Lee, K. B.; Moehl, T.; Marchioro, A.; Moon, S. J.; Humphry-Baker, R.; Yum, J. H.; Moser, J. E. et al. Lead iodide perovskite sensitized all-solid-state submicron thin film mesoscopic solar cell with efficiency exceeding 9%. *Sci. Rep.* **2012**, *2*, 591.

[4] Yang, W. S.; Noh, J. H.; Jeon, N. J.; Kim, Y. C.; Ryu, S.; Seo, J.; Seok, S. I. High-performance photovoltaic perovskite layers fabricated through intramolecular exchange. *Science* **2015**, *348*, 1234–1237.

[5] Bai, S.; Wu, Z. W.; Wu, X. J.; Jin, Y. Z.; Zhao, N.; Chen, Z. H.; Mei, Q. Q.; Wang, X.; Ye, Z. Z.; Song, T. et al. High-performance planar heterojunction perovskite solar cells: Preserving long charge carrier diffusion lengths and interfacial engineering. *Nano Res.* **2014**, *7*, 1749–1758.

[6] Kojima, A.; Teshima, K.; Shirai, Y.; Miyasaka, T. Organometal halide perovskites as visible-light sensitizers for photovoltaic cells. *J. Am. Chem. Soc.* **2009**, *131*, 6050–6051.

[7] Jeon, N. J.; Noh, J. H.; Kim, Y. C.; Yang, W. S.; Ryu, S.; Seok, S. I. Solvent engineering for high-performance inorganic–organic hybrid perovskite solar cells. *Nat. Mater.* **2014**, *13*, 897–903.

[8] Bi, D. Q.; Yi, C. Y.; Luo, J. S.; Décoppet, J. D.; Zhang, F.; Zakeeruddin, S. M.; Li, X.; Hagfeldt, A.; Grätzel, M. Polymer-templated nucleation and crystal growth of perovskite films for solar cells with efficiency greater than 21%. *Nat. Energy* **2016**, *1*, 16142.

[9] Tan, H. R.; Jain, A.; Voznyy, O.; Lan, X. Z.; GarcÍa de Arquer, F. P.; Fan, J. Z.; Quintero-Bermudez, R.; Yuan, M. J.; Zhang, B.; Zhao, Y. C. et al. Efficient and stable solution-processed planar perovskite solar cells via contact passivation. *Science* **2017**, *355*, 722–726.

[10] Jeon, N. J.; Na, H.; Jung, E. H.; Yang, T. Y.; Lee, Y. G.; Kim, G.; Shin, H. W.; Seok, S. I.; Lee, J.; Seo, J. A fluorene-terminated hole-transporting material for highly efficient and stable perovskite solar cells. *Nat. Energy* **2018**, *3*, 682–689.

[11] Jeong, M.; Choi, I. W.; Go, E. M.; Cho, Y.; Kim, M.; Lee, B.; Jeong, S.; Jo, Y.; Choi, H. W.; Lee, J. et al. Stable perovskite solar cells with efficiency exceeding 24.8% and 0.3-V voltage loss. *Science* **2020**, *369*, 1615–1620.

[12] Yoo, J. J.; Seo, G.; Chua, M. R.; Park, T. G.; Lu, Y. L.; Rotermund, F.; Kim, Y. K.; Moon, C. S.; Jeon, N. J.; Correa-Baena, J. P. et al. Efficient perovskite solar cells via improved carrier management. *Nature* **2021**, *590*, 587–593.

[13] Tu, Y. G.; Xu, G. N.; Yang, X. Y.; Zhang, Y. F.; Li, Z. J.; Su, R.; Luo, D. Y.; Yang, W. Q.; Miao, Y.; Cai, R. et al. Mixed-cation perovskite solar cells in space. *Sci. China Phys. Mech. Astron.* **2019**, *62*, 974221.

[14] Yang, J. M.; Bao, Q. Y.; Shen, L.; Ding, L. M. Potential applications for perovskite solar cells in space. *Nano Energy* **2020**, *76*, 105019.

[15] Li, X.; Du, J. Y.; Duan, H.; Wang, H. Y.; Fan, L.; Sun, Y. F.; Sui, Y. R.; Yang, J. H.; Wang, F. Y.; Yang, L. L. Moisture-preventing $MAPbI_3$ solar cells with high photovoltaic performance via multiple ligand engineering. *Nano Res.* **2022**, *15*, 1375–1382.

[16] Tu, Y. G.; Wu, J.; Xu, G. N.; Yang, X. Y.; Cai, R.; Gong, Q. H.; Zhu, R.; Huang, W. Perovskite solar cells for space applications: Progress and challenges. *Adv. Mater.* **2021**, *33*, 2006545.

[17] Zhao, X. ; Fang, W. H. ; Long, R. ; Prezhdo, O. V. Chemical passivation of methylammonium fragments eliminates traps, extends charge lifetimes, and restores structural stability of

$CH_3NH_3PbI_3$ perovskite. *Nano Res.*, in press, https://doi.org/10.1007/s12274-021-4054-z.

[18] Wang, F. Y.; Yang, M. F.; Zhang, Y. H.; Du, J. Y.; Yang, S.; Yang, L. L.; Fan, L.; Sui, Y. R.; Sun, Y. F.; Yang, J. H. Full-scale chemical and field-effect passivation: 21.52% efficiency of stable $MAPbI_3$ solar cells via benzenamine modification. *Nano Res.* **2021**, *14*, 2783–2789.

[19] Sha, W. E. I.; Ren, X. G.; Chen, L. Z.; Choy, W. C. H. The efficiency limit of $CH_3NH_3PbI_3$ perovskite solar cells. *Appl. Phys. Lett.* **2015**, *106*, 221104.

[20] Zhou, H. P.; Chen, Q.; Li, G.; Luo, S.; Song, T. B.; Duan, H. S.; Hong, Z. R.; You, J. B.; Liu, Y. S.; Yang, Y. Interface engineering of highly efficient perovskite solar cells. *Science* **2014**, *345*, 542–546.

[21] Jeon, N. J.; Noh, J. H.; Yang, W. S.; Kim, Y. C.; Ryu, S.; Seo, J.; Seok, S. I. Compositional engineering of perovskite materials for high-performance solar cells. *Nature* **2015**, *517*, 476–480.

[22] Da, P. M.; Zheng, G. F. Tailoring interface of lead-halide perovskite solar cells. *Nano Res.* **2017**, *10*, 1471–1497.

[23] Cho, A. N.; Park, N. G. Impact of interfacial layers in perovskite solar cells. *ChemSusChem* **2017**, *10*, 3687–3704.

[24] Hou, Y.; Du, X. Y.; Scheiner, S.; McMeekin, D. P.; Wang, Z. P.; Li, N.; Killian, M. S.; Chen, H. W.; Richter, M.; Levchuk, I. et al. A generic interface to reduce the efficiency-stability-cost gap of perovskite solar cells. *Science* **2017**, *358*, 1192–1197.

[25] Yang, W. S.; Park, B. W.; Jung, E. H.; Jeon, N. J.; Kim, Y. C.; Lee, D. U.; Shin, S. S.; Seo, J.; Kim, E. K.; Noh, J. H. et al. Iodide management in formamidinium-lead-halide-based perovskite layers for efficient solar cells. *Science* **2017**, *356*, 1376–1379.

[26] Zhang, F.; Zhu, K. Additive engineering for efficient and stable perovskite solar cells. *Adv. Energy Mater.* **2020**, *10*, 1902579.

[27] Liu, K. K.; Xie, L. Q.; Song, P. Q.; Lin, K. B.; Shen, L. N.; Liang, Y. M.; Lu, J. X.; Feng, W. J.; Guan, X.; Yan, C. Z. et al. Stable perovskite solar cells enabled by simultaneous surface and bulk defects passivation. *Sol. RRL* **2020**, *4*, 2000224.

[28] Mei, A. Y.; Sheng, Y. S.; Ming, Y.; Hu, Y.; Rong, Y. G.; Zhang, W. H.; Luo, S. L.; Na, G.; Tian, C. B.; Hou, X. M. et al. Stabilizing perovskite solar cells to IEC61215: 2016 standards with over 9, 000-h operational tracking. *Joule* **2020**, *4*, 2646–2660.

[29] Kim, M.; Jeong, J.; Lu, H.; Lee Tae, K.; Eickemeyer Felix, T.; Liu, Y.; Choi In, W.; Choi Seung, J.; Jo, Y.; Kim, H.-B. et al. Conformal quantum dot-SnO_2 layers as electron transporters for efficient perovskite solar cells. *Science* **2022**, *375*, 302–306.

[30] Yu, W. J.; Sun, X. R.; Xiao, M.; Hou, T.; Liu, X.; Zheng, B. L.; Yu, H.; Zhang, M.; Huang, Y. L.; Hao, X. J. Recent advances on interface engineering of perovskite solar cells. *Nano Res.* **2022**, *15*, 85–103.

[31] Fang, Y. J.; Bi, C.; Wang, D.; Huang, J. S. The functions of fullerenes in hybrid perovskite solar cells. *ACS Energy Lett.* **2017**, *2*, 782–794.

[32] Zhang, M.; Lyu, M.; Yun, J. H.; Noori, M.; Zhou, X. J.; Cooling, N. A.; Wang, Q.; Yu, H.; Dastoor, P. C.; Wang, L. Z. Low-temperature processed solar cells with formamidinium tin halide perovskite/fullerene heterojunctions. *Nano Res.* **2016**, *9*, 1570–1577.

[33] Zheng, X. P.; Hou, Y.; Bao, C. X.; Yin, J.; Yuan, F. L.; Huang, Z. R.; Song, K. P.; Liu, J. K.; Troughton, J.; Gasparini, N. et al. Managing grains and interfaces via ligand anchoring enables 22.3%-efficiency inverted perovskite solar cells. *Nat. Energy* **2020**, *5*, 131–140.

[34] Jia, L. B.; Zhang, L. X.; Ding, L. M.; Yang, S. F. Using fluorinated and crosslinkable fullerene derivatives to improve the stability of perovskite solar cells. *J. Semicond.* **2021**, *42*, 120201.

[35] Ke, W. J.; Zhao, D. W.; Grice, C. R.; Cimaroli, A. J.; Ge, J.; Tao, H.; Lei, H. W.; Fang, G. J.; Yan, Y. F. Efficient planar perovskite solar cells using room-temperature vacuum-processed C_{60} electron selective layers. *J. Mater. Chem. A* **2015**, *3*, 17971–17976.

[36] Collavini, S.; Kosta, I.; Völker, S. F.; Cabanero, G.; Grande, H. J.; Tena-Zaera, R.; Delgado, J. L. Efficient regular perovskite solar cells based on pristine [70]fullerene as electron-selective contact. *ChemSusChem* **2016**, *9*, 1263–1270.

[37] Wang, Y. C.; Li, X. D.; Zhu, L. P.; Liu, X. H.; Zhang, W. J.; Fang, J. F. Efficient and hysteresis-free perovskite solar cells based on a solution processable polar fullerene electron transport layer. *Adv. Energy Mater.* **2017**, *7*, 1701144.

[38] Xie, J. S.; Yu, X. G.; Huang, J. B.; Sun, X.; Zhang, Y. H.; Yang, Z. R.; Lei, M.; Xu, L. B.; Tang, Z. G.; Cui, C. et al. Self-organized fullerene interfacial layer for efficient and low-temperature processed planar perovskite solar cells with high UV-light stability. *Adv. Sci.* **2017**, *4*, 1700018.

[39] Cao, T. T.; Chen, K.; Chen, Q. Y.; Zhou, Y.; Chen, N.; Li, Y. F. Fullerene derivative-modified SnO_2 electron transport layer for highly efficient perovskite solar cells with efficiency over 21%. *ACS Appl. Mater. Interfaces* **2019**, *11*, 33825–33834.

[40] Castro, E.; Murillo, J.; Fernandez-Delgado, O.; Echegoyen, L. Progress in fullerene-based hybrid perovskite solar cells. *J. Mater. Chem. C* **2018**, *6*, 2635–2651.

[41] Collavini, S.; Saliba, M.; Tress, W. R.; Holzhey, P. J.; Völker, S. F.; Domanski, K.; Turren-Cruz, S. H.; Ummadisingu, A.; Zakeeruddin, S. M.; Hagfeldt, A. et al. Poly(ethylene glycol)-[60]fullerene-based materials for perovskite solar cells with improved moisture resistance and reduced hysteresis. *ChemSusChem* **2018**, *11*, 1032–1039.

[42] Wang, S. H.; Chen, H. Y.; Zhang, J. D.; Xu, G. Y.; Chen, W. J.; Xue, R. M.; Zhang, M. Y.; Li, Y. W.; Li, Y. F. Targeted therapy for interfacial engineering toward stable and efficient perovskite solar cells. *Adv. Mater.* **2019**, *31*, 1903691.

[43] Shao, Y. C.; Yuan, Y. B.; Huang, J. S. Correlation of energy disorder and open-circuit voltage in hybrid perovskite solar cells. *Nat. Energy* **2016**, *1*, 15001.

[44] Liang, P. W.; Chueh, C. C.; Williams, S. T.; Jen, A. K. Y. Roles of fullerene-based interlayers in enhancing the performance of organometal perovskite thin-film solar cells. *Adv. Energy Mater.* **2015**, *5*, 1402321.

[45] Liang, Y. M.; Song, P. Q.; Tian, H. R.; Tian, C. B.; Tian, W. J.; Nan, Z. A.; Cai, Y. T.; Yang, P. P.; Sun, C.; Chen, J. F. et al. Lead leakage preventable fullerene-porphyrin dyad for efficient and stable perovskite solar cells. *Adv. Funct. Mater.*, in press, https://doi.org/10.1002/adfm.202110139.

[46] Li, X. D.; Zhang, W. X.; Guo, X. M.; Lu, C. Y.; Wei, J. Y.; Fang, J. F. Constructing heterojunctions by surface sulfidation for efficient inverted perovskite solar cells. *Science* **2022**, *375*, 434–437.

[47] Kan, C. X.; Tang, Z. F.; Yao, Y. X.; Hang, P. J.; Li, B.; Wang, Y.; Sun, X.; Lei, M.; Yang, D. R.; Yu, X. G. Mitigating ion migration by polyethylene glycol-modified fullerene for perovskite solar cells with enhanced stability. *ACS Energy Lett.* **2021**, *6*, 3864–3872.

[48] Li, C. Z.; Chueh, C. C.; Yip, H. L.; Ding, F. Z.; Li, X. S.; Jen, A. K. Y. Solution-processible highly conducting fullerenes. *Adv. Mater.* **2013**, *25*, 2457–2461.

[49] Jeng, J. Y.; Chiang, Y. F.; Lee, M. H.; Peng, S. R.; Guo, T. F.; Chen, P.; Wen, T. C. $CH_3NH_3PbI_3$ perovskite/fullerene planar-heterojunction hybrid solar cells. *Adv. Mater.* **2013**, *25*, 3727–3732.

[50] Heo, J. H.; Han, H. J.; Kim, D.; Ahn, T. K.; Im, S. H. Hysteresis-less inverted $CH_3NH_3PbI_3$ planar perovskite hybrid solar cells with 18.1% power conversion efficiency. *Energy Environ. Sci.* **2015**, *8*, 1602–1608.

[51] Wolff, C. M.; Zu, F. S.; Paulke, A.; Toro, L. P.; Koch, N.; Neher, D. Reduced interface-mediated recombination for high open-circuit voltages in $CH_3NH_3PbI_3$ solar cells. *Adv. Mater.* **2017**, *29*, 1700159.

[52] Shao, Y. C.; Xiao, Z. G.; Bi, C.; Yuan, Y. B.; Huang, J. S. Origin and elimination of photocurrent hysteresis by fullerene passivation in $CH_3NH_3PbI_3$ planar heterojunction solar cells. *Nat. Commun.* **2014**, *5*, 5784.

[53] Bai, Y.; Dong, Q. F.; Shao, Y. C.; Deng, Y. H.; Wang, Q.; Shen, L.; Wang, D.; Wei, W.; Huang, J. S. Enhancing stability and efficiency of perovskite solar cells with crosslinkable silane-functionalized and doped fullerene. *Nat. Commun.* **2016**, *7*, 12806.

[54] Meng, L.; You, J. B.; Guo, T. F.; Yang, Y. Recent advances in the inverted planar structure of perovskite solar cells. *Acc. Chem. Res.* **2016**, *49*, 155–165.

[55] Deng, L. L.; Xie, S. Y.; Gao, F. Fullerene-based materials for

photovoltaic applications: Toward efficient, hysteresis-free, and stable perovskite solar cells. *Adv. Electron. Mater.* **2018**, *4*, 1700435.

[56] Pascual, J.; Delgado, J. L.; Tena-Zaera, R. Physicochemical phenomena and application in solar cells of perovskite: Fullerene films. *J. Phys. Chem. Lett.* **2018**, *9*, 2893–2902.

[57] Docampo, P.; Ball, J. M.; Darwich, M.; Eperon, G. E.; Snaith, H. J. Efficient organometal trihalide perovskite planar-heterojunction solar cells on flexible polymer substrates. *Nat. Commun.* **2013**, *4*, 2761.

[58] Cao, T. T.; Huang, P.; Zhang, K. C.; Sun, Z. Q.; Zhu, K.; Yuan, L. G.; Chen, K.; Chen, N.; Li, Y. F. Interfacial engineering via inserting functionalized water-soluble fullerene derivative interlayers for enhancing the performance of perovskite solar cells. *J. Mater. Chem. A* **2018**, *6*, 3435–3443.

[59] Xing, Y.; Sun, C.; Yip, H. L.; Bazan, G. C.; Huang, F.; Cao, Y. New fullerene design enables efficient passivation of surface traps in high performance p–i–n heterojunction perovskite solar cells. *Nano Energy* **2016**, *26*, 7–15.

[60] Dai, S. M.; Zhang, X.; Chen, W. Y.; Li, X.; Tan, Z. A.; Li, C.; Deng, L. L.; Zhan, X. X.; Lin, M. S.; Xing, Z. et al. Formulation engineering for optimizing ternary electron acceptors exemplified by isomeric $PC_{71}BM$ in planar perovskite solar cells. *J. Mater. Chem. A* **2016**, *4*, 18776–18782.

[61] Xu, J. X.; Buin, A.; Ip, A. H.; Li, W.; Voznyy, O.; Comin, R.; Yuan, M. J.; Jeon, S.; Ning, Z. J.; McDowell, J. J. et al. Perovskite-fullerene hybrid materials suppress hysteresis in planar diodes. *Nat. Commun.* **2015**, *6*, 7081.

[62] Tian, C. B.; Castro, E.; Betancourt-Solis, G.; Nan, Z. A.; Fernandez-Delgado, O.; Jankuru, S.; Echegoyen, L. Fullerene derivative with a branched alkyl chain exhibits enhanced charge extraction and stability in inverted planar perovskite solar cells. *New J. Chem.* **2018**, *42*, 2896–2902.

[63] Chiang, C. H.; Wu, C. G. Bulk heterojunction perovskite-PCBM solar cells with high fill factor. *Nat. Photonics* **2016**, *10*, 196–200.

[64] Wu, Y. Z.; Yang, X. D.; Chen, W.; Yue, Y. F.; Cai, M. L.; Xie, F. X.; Bi, E. B.; Islam, A.; Han, L. Perovskite solar cells with 18.21% efficiency and area over 1 cm^2 fabricated by heterojunction engineering. *Nat. Energy* **2016**, *1*, 16148.

[65] Zhang, F.; Shi, W. D.; Luo, J. S.; Pellet, N.; Yi, C. Y.; Li, X.; Zhao, X. M.; Dennis, T. J. S.; Li, X. G.; Wang, S. R. et al. Isomer-pure bis-PCBM-assisted crystal engineering of perovskite solar cells showing excellent efficiency and stability. *Adv. Mater.* **2017**, *29*, 1606806.

[66] Li, Y. W.; Zhao, Y.; Chen, Q.; Yang, Y.; Liu, Y. S.; Hong, Z. R.; Liu, Z. H.; Hsieh, Y. T.; Meng, L.; Li, Y. F. et al. Multifunctional fullerene derivative for interface engineering in perovskite solar cells. *J. Am. Chem. Soc.* **2015**, *137*, 15540–15547.

[67] Dong, Q.; Ho, C. H. Y.; Yu, H.; Salehi, A.; So, F. Defect passivation by fullerene derivative in perovskite solar cells with aluminum-doped zinc oxide as electron transporting layer. *Chem. Mater.* **2019**, *31*, 6833–6840.

[68] Luo, Z. H.; Wu, F.; Zhang, T.; Zeng, X.; Xiao, Y. Q.; Liu, T.; Zhong, C.; Lu, X. H.; Zhu, L. N.; Yang, S. H. et al. Designing a perylene diimide/fullerene hybrid as effective electron transporting material in inverted perovskite solar cells with enhanced efficiency and stability. *Angew. Chem., Int. Ed.* **2019**, *58*, 8520–8525.

[69] Bertoluzzi, L.; Belisle, R. A.; Bush, K. A.; Cheacharoen, R.; McGehee, M. D.; O'Regan, B. C. *In situ* measurement of electric-field screening in hysteresis-free PTAA/$FA_{0.83}Cs_{0.17}Pb(I_{0.83}Br_{0.17})_3$/$C_{60}$ perovskite solar cells gives an ion mobility of ~ 3×10^{-7} $cm^2/(V \cdot s)$, 2 orders of magnitude faster than reported for metal-oxide-contacted perovskite cells with hysteresis. *J. Am. Chem. Soc.* **2018**, *140*, 12775–12784.

[70] Huang, H. H.; Tsai, H.; Raja, R.; Lin, S. L.; Ghosh, D.; Hou, C. H.; Shyue, J. J.; Tretiak, S.; Chen, W.; Lin, K. F. et al. Robust unencapsulated perovskite solar cells protected by a fluorinated fullerene electron transporting layer. *ACS Energy Lett.* **2021**, *6*, 3376–3385.

[71] Zhou, Y. Q.; Wu, B. S.; Lin, G. H.; Xing, Z.; Li, S. H.; Deng, L. L.; Chen, D. C.; Yun, D. Q.; Xie, S. Y. Interfacing pristine C_{60} onto TiO_2 for viable flexibility in perovskite solar cells by a low-temperature all-solution process. *Adv. Energy Mater.* **2018**, *8*, 1800399.

[72] Xu, G. Y.; Wang, S. H.; Bi, P. Q.; Chen, H. Y.; Zhang, M. Y.; Xue, R. M.; Hao, X. T.; Wang, Z. K.; Li, Y. W.; Li, Y. F. Hydrophilic fullerene derivative doping in active layer and electron transport layer for enhancing oxygen stability of perovskite solar cells. *Sol. RRL* **2020**, *4*, 1900249.

[73] Aristidou, N.; Eames, C.; Sanchez-Molina, I.; Bu, X. N.; Kosco, J.; Islam, M. S.; Haque, S. A. Fast oxygen diffusion and iodide defects mediate oxygen-induced degradation of perovskite solar cells. *Nat. Commun.* **2017**, *8*, 15218.

[74] Gatti, T.; Menna, E.; Meneghetti, M.; Maggini, M.; Petrozza, A.; Lamberti, F. The renaissance of fullerenes with perovskite solar cells. *Nano Energy* **2017**, *41*, 84–100.

[75] Elnaggar, M.; Elshobaki, M.; Mumyatov, A.; Luchkin, S. Y.; Dremova, N. N.; Stevenson, K. J.; Troshin, P. A. Molecular engineering of the fullerene-based electron transport layer materials for improving ambient stability of perovskite solar cells. *Sol. RRL* **2019**, *3*, 1900223.

[76] Jia, L. B.; Chen, M. Q.; Yang, S. F. Functionalization of fullerene materials toward applications in perovskite solar cells. *Mater. Chem. Front.* **2020**, *4*, 2256–2282.

[77] Fernandez-Delgado, O.; Castro, E.; Ganivet, C. R.; Fosnacht, K.; Liu, F.; Mates, T.; Liu, Y.; Wu, X. J.; Echegoyen, L. Variation of interfacial interactions in $PC_{61}BM$-like electron-transporting compounds for perovskite solar cells. *ACS Appl. Mater. Interfaces* **2019**, *11*, 34408–34415.

[78] Taufique, M. F. N.; Mortuza, S. M.; Banerjee, S. Mechanistic insight into the attachment of fullerene derivatives on crystal faces of methylammonium lead iodide based perovskites. *J. Phys. Chem. C* **2016**, *120*, 22426–22432.

[79] Xing, Z.; Li, S. H.; Hui, Y.; Wu, B. S.; Chen, Z. C.; Yun, D. Q.; Deng, L. L.; Zhang, M. L.; Mao, B. W.; Xie, S. Y. et al. Star-like hexakis[di(ethoxycarbonyl)methano]-C_{60} with higher electron mobility: An unexpected electron extractor interfaced in photovoltaic perovskites. *Nano Energy* **2020**, *74*, 104859.

[80] Tian, C. B.; Castro, E.; Wang, T.; Betancourt-Solis, G.; Rodriguez, G.; Echegoyen, L. Improved performance and stability of inverted planar perovskite solar cells using fulleropyrrolidine layers. *ACS Appl. Mater. Interfaces* **2016**, *8*, 31426–31432.

[81] Tian, C. B.; Zhang, S. J.; Mei, A. Y.; Rong, Y. G.; Hu, Y.; Du, K.; Duan, M.; Sheng, Y. S.; Jiang, P.; Xu, G. Z. et al. A multifunctional bis-adduct fullerene for efficient printable mesoscopic perovskite solar cells. *ACS Appl. Mater. Interfaces* **2018**, *10*, 10835–10841.

[82] Tian, C. B.; Kochiss, K.; Castro, E.; Betancourt-Solis, G.; Han, H. W.; Echegoyen, L. A dimeric fullerene derivative for efficient inverted planar perovskite solar cells with improved stability. *J. Mater. Chem. A* **2017**, *5*, 7326–7332.

[83] Tian, C. B.; Lin, K.; Lu, J.; Feng, W.; Song, P.; Xie, L.; Wei, Z. Interfacial bridge using a cis-fulleropyrrolidine for efficient planar perovskite solar cells with enhanced stability. *Small Methods* **2019**, *4*, 1900476.

[84] Noel, N. K.; Abate, A.; Stranks, S. D.; Parrott, E. S.; Burlakov, V. M.; Goriely, A.; Snaith, H. J. Enhanced photoluminescence and solar cell performance via lewis base passivation of organic–inorganic lead halide perovskites. *ACS Nano* **2014**, *8*, 9815–9821.

[85] Liu, H. R.; Li, S. H.; Deng, L. L.; Wang, Z. Y.; Xing, Z.; Rong, X.; Tian, H. R.; Li, X.; Xie, S. Y.; Huang, R. B. et al. Pyridine-functionalized fullerene electron transport layer for efficient planar perovskite solar cells. *ACS Appl. Mater. Interfaces* **2019**, *11*, 23982–23989.

[86] Li, B. R.; Zhen, J. M.; Wan, Y. Y.; Lei, X. Y.; Liu, Q.; Liu, Y. J.; Jia, L. B.; Wu, X. J.; Zeng, H. L.; Zhang, W. F. et al. Anchoring fullerene onto perovskite film via grafting pyridine toward enhanced electron transport in high-efficiency solar cells. *ACS Appl. Mater. Interfaces* **2018**, *10*, 32471–32482.

[87] Li, B. R.; Zhen, J. M.; Wan, Y. Y.; Lei, X. Y.; Jia, L. B.; Wu, X. J.;

Zeng, H. L.; Chen, M. Q.; Wang, G. W.; Yang, S. F. Steering the electron transport properties of pyridine-functionalized fullerene derivatives in inverted perovskite solar cells: The nitrogen site matters. *J. Mater. Chem. A* **2020**, *8*, 3872–3881.

[88] Liu, X.; Lin, F.; Chueh, C. C.; Chen, Q.; Zhao, T.; Liang, P. W.; Zhu, Z. L.; Sun, Y.; Jen, A. K. Y. Fluoroalkyl-substituted fullerene/perovskite heterojunction for efficient and ambient stable perovskite solar cells. *Nano Energy* **2016**, *30*, 417–425.

[89] Unger, E. L.; Hoke, E. T.; Bailie, C. D.; Nguyen, W. H.; Bowring, A. R.; Heumüller, T.; Christoforo, M. G.; McGehee, M. D. Hysteresis and transient behavior in current–voltage measurements of hybrid-perovskite absorber solar cells. *Energy Environ. Sci.* **2014**, *7*, 3690–3698.

[90] Wang, H.; Li, F. B.; Wang, P.; Sun, R.; Ma, W.; Chen, M. T.; Miao, W. Q.; Liu, D.; Wang, T. Chlorinated fullerene dimers for interfacial engineering toward stable planar perovskite solar cells with 22.3% efficiency. *Adv. Energy Mater.* **2020**, *10*, 2000615.

[91] Zhang, M. Y.; Chen, Q.; Xue, R. M.; Zhan, Y.; Wang, C.; Lai, J. Q.; Yang, J.; Lin, H. Z.; Yao, J. L.; Li, Y. W. et al. Reconfiguration of interfacial energy band structure for high-performance inverted structure perovskite solar cells. *Nat. Commun.* **2019**, *10*, 4593.

[92] Sandoval-Torrientes, R.; Pascual, J.; García-Benito, I.; Collavini, S.; Kosta, I.; Tena-Zaera, R.; Martín, N.; Delgado, J. L. Modified fullerenes for efficient electron transport layer-free perovskite/fullerene blend-based solar cells. *ChemSusChem* **2017**, *10*, 2023–2029.

[93] Pascual, J.; Collavini, S.; Völker, S. F.; Phung, N.; Palacios-Lidon, E.; Irusta, L.; Grande, H. J.; Abate, A.; Tena-Zaera, R.; Delgado, J. L. Unravelling fullerene-perovskite interactions introduces advanced blend films for performance-improved solar cells. *Sustainable Energy Fuels* **2019**, *3*, 2779–2787.

[94] Wang, X.; Rakstys, K.; Jack, K.; Jin, H.; Lai, J.; Li, H.; Ranasinghe, C. S. K.; Saghaei, J.; Zhang, G. R.; Burn, P. L. et al. Engineering fluorinated-cation containing inverted perovskite solar cells with an efficiency of > 21% and improved stability towards humidity. *Nat. Commun.* **2021**, *12*, 52.

[95] Rajagopal, A.; Liang, P. W.; Chueh, C. C.; Yang, Z. B.; Jen, A. K. Y. Defect passivation via a graded fullerene heterojunction in low-bandgap Pb-Sn binary perovskite photovoltaics. *ACS Energy Lett.* **2017**, *2*, 2531–2539.

[96] Chang, C. Y.; Wang, C. P.; Raja, R.; Wang, L.; Tsao, C. S.; Su, W. F. High-efficiency bulk heterojunction perovskite solar cell fabricated by one-step solution process using single solvent: Synthesis and characterization of material and film formation mechanism. *J. Mater. Chem. A* **2018**, *6*, 4179–4188.

[97] Abrusci, A.; Stranks, S. D.; Docampo, P.; Yip, H. L.; Jen, A. K. Y.; Snaith, H. J. High-performance perovskite-polymer hybrid solar cells via electronic coupling with fullerene monolayers. *Nano Lett.* **2013**, *13*, 3124–3128.

[98] Dong, Y.; Li, W. H.; Zhang, X. J.; Xu, Q.; Liu, Q.; Li, C. H.; Bo, Z. S. Highly efficient planar perovskite solar cells via interfacial modification with fullerene derivatives. *Small* **2016**, *12*, 1098–1104.

[99] Wang, H.; Cai, F. L.; Zhang, M.; Wang, P.; Yao, J. X.; Gurney, R. S.; Li, F. B.; Liu, D.; Wang, T. Halogen-substituted fullerene derivatives for interface engineering of perovskite solar cells. *J. Mater. Chem. A* **2018**, *6*, 21368–21378.

[100] Zhong, M. Y.; Liang, Y. Q.; Zhang, J. Q.; Wei, Z. X.; Li, Q.; Xu, D. S. Highly efficient flexible $MAPbI_3$ solar cells with a fullerene derivative-modified SnO_2 layer as the electron transport layer. *J. Mater. Chem. A* **2019**, *7*, 6659–6664.

[101] Yang, Z. J.; Zhong, M. Y.; Liang, Y. Q.; Yang, L. W.; Liu, X. Y.; Li, Q.; Zhang, J.; Xu, D. S. SnO_2-C_{60} pyrrolidine tris-acid (CPTA) as the electron transport layer for highly efficient and stable planar Sn-based perovskite solar cells. *Adv. Funct. Mater.* **2019**, *29*, 1903621.

[102] Wang, J. K.; Datta, K.; Weijtens, C. H. L.; Wienk, M. M.; Janssen, R. A. J. Insights into fullerene passivation of SnO_2 electron transport layers in perovskite solar cells. *Adv. Funct. Mater.* **2019**, *29*, 1905883.

[103] Liu, K.; Chen, S.; Wu, J. H.; Zhang, H. Y.; Qin, M. C.; Lu, X. H.; Tu, Y. F.; Meng, Q. B.; Zhan, X. W. Fullerene derivative anchored SnO_2 for high-performance perovskite solar cells. *Energy Environ. Sci.* **2018**, *11*, 3463–3471.

[104] Xu, G. Y.; Xue, R. M.; Chen, W. J.; Zhang, J. W.; Zhang, M. Y.; Chen, H. Y.; Cui, C. H.; Li, H. K.; Li, Y. W.; Li, Y. F. New strategy for two-step sequential deposition: Incorporation of hydrophilic fullerene in second precursor for high-performance p–i–n planar perovskite solar cells. *Adv. Energy Mater.* **2018**, *8*, 1703054.

[105] Yao, K.; Leng, S. F.; Liu, Z. L.; Fei, L. F.; Chen, Y. J.; Li, S. B.; Zhou, N. G.; Zhang, J.; Xu, Y. X.; Zhou, L. et al. Fullerene-anchored core–shell ZnO nanoparticles for efficient and stable dual-sensitized perovskite solar cells. *Joule* **2019**, *3*, 417–431.

[106] Jie, Z.; Leyu, B.; Yuanhang, C.; Baomin, X.; Alex K.-Y, J. Self-assembled monolayer enabling improved buried interfaces in blade-coated perovskite solar cells for high efficiency and stability. *Nano Research Energy*, in press, https://doi.org/10.26599/NRE.2022.9120004.

[107] Kim, J.; Kim, G.; Kim, T. K.; Kwon, S.; Back, H.; Lee, J.; Lee, S. H.; Kang, H.; Lee, K. Efficient planar-heterojunction perovskite solar cells achieved via interfacial modification of a sol-gel ZnO electron collection layer. *J. Mater. Chem. A* **2014**, *2*, 17291–17296.

[108] Li, S. H.; Xing, Z.; Wu, B. S.; Chen, Z. C.; Yao, Y. R.; Tian, H. R.; Li, M. F.; Yun, D. Q.; Deng, L. L.; Xie, S. Y. et al. Hybrid fullerene-based electron transport layers improving the thermal stability of perovskite solar cells. *ACS Appl. Mater. Interfaces* **2020**, *12*, 20733–20740.

[109] Xing, Z.; Li, S. H.; Xie, F. F.; Xu, P. Y.; Deng, L. L.; Zhong, X. X.; Xie, S. Y. Mixed fullerene electron transport layers with fluorocarbon chains assembling on the surface: A moisture-resistant coverage for perovskite solar cells. *ACS Appl. Mater. Interfaces* **2020**, *12*, 35081–35087.

[110] Tian, C. B.; Betancourt-Solis, G.; Nan, Z.; Liu, K. K.; Lin, K. B.; Lu, J. X.; Xie, L. Q.; Echegoyen, L.; Wei, Z. H. Efficient and stable inverted perovskite solar cells enabled by inhibition of self-aggregation of fullerene electron-transporting compounds. *Sci. Bull.* **2021**, *66*, 339–346.

[111] Wojciechowski, K.; Ramirez, I.; Gorisse, T.; Dautel, O.; Dasari, R.; Sakai, N.; Hardigree, J. M.; Song, S.; Marder, S.; Riede, M. et al. Cross-linkable fullerene derivatives for solution-processed n–i–p perovskite solar cells. *ACS Energy Lett.* **2016**, *1*, 648–653.

[112] Tao, C.; Van Der Velden, J.; Cabau, L.; Montcada, N. F.; Neutzner, S.; Srimath Kandada, A. R.; Marras, S.; Brambilla, L.; Tommasini, M.; Xu, W. D. et al. Fully solution-processed n–i–p-like perovskite solar cells with planar junction: How the charge extracting layer determines the open-circuit voltage. *Adv. Mater.* **2017**, *29*, 1604493.

[113] Kang, T.; Tsai, C. M.; Jiang, Y. H.; Gollavelli, G.; Mohanta, N.; Diau, E. W. G.; Hsu, C. S. Interfacial engineering with cross-linkable fullerene derivatives for high-performance perovskite solar cells. *ACS Appl. Mater. Interfaces* **2017**, *9*, 38530–38536.

[114] Watson, B. L.; Rolston, N.; Bush, K. A.; Leijtens, T.; McGehee, M. D.; Dauskardt, R. H. Cross-linkable, solvent-resistant fullerene contacts for robust and efficient perovskite solar cells with increased J_{SC} and V_{OC}. *ACS Appl. Mater. Interfaces* **2016**, *8*, 25896–25904.

[115] Song, S.; Hill, R.; Choi, K.; Wojciechowski, K.; Barlow, S.; Leisen, J.; Snaith, H. J.; Marder, S. R.; Park, T. Surface modified fullerene electron transport layers for stable and reproducible flexible perovskite solar cells. *Nano Energy* **2018**, *49*, 324–332.

[116] Li, M.; Yang, Y. G.; Wang, Z. K.; Kang, T.; Wang, Q.; Turren-Cruz, S. H.; Gao, X. Y.; Hsu, C. S.; Liao, L. S.; Abate, A. Perovskite grains embraced in a soft fullerene network make highly efficient flexible solar cells with superior mechanical stability. *Adv. Mater.* **2019**, *31*, 1901519.